Authors: M. Pedrotti* and A. Tarantino*

Affiliation: *Department of Civil and Environmental Engineering, University of Strathclyde, Glasgow, Scotland, UK.

Corresponding author: M. Pedrotti, Department of Civil and Environmental Engineering, University of Strathclyde, James Weir Building - Level 5, 75 Montrose Street - Glasgow G1 1XJ, Scotland, UK.

E-mail: matteo.pedrotti@strath.ac.uk

Abstract

Reconstituted and compacted soils are commonly assumed to exhibit a fundamentally different behaviour due to different microstructure. However, inspection of pore size distribution of the same soil in compacted and reconstituted states suggests that the boundary between these two states is more blurred. This paper explores the continuity between the microstructure of reconstituted and compacted states of kaolin clay and formulates a conceptual constitutive model unifying these states. Clay samples were prepared by saturating the pore space with different fluids (water, acetone, and air) and the effect of pore-fluid fraction on the micro- and macroscale response of the clay was investigated experimentally. A conceptual constitutive model for unsaturated clays for quasi-isotropic stress states was therefore formulated, which allows modelling various unsaturated hydro-mechanical paths based on constitutive parameters only derived from the compression behaviour of clay under dry and saturated conditions (testing on samples formed from dry powder and slurry respectively).

INTRODUCTION

Soil microstructure is often the key to interpret major aspects of hydro-mechanical response of unsaturated (compacted) soils. Implicit or explicit microstructural assumptions have been used to inform mechanical constitutive models (Gallipoli et al., 2003, Wheeler et al., 2003, Tarantino, 2007, Alonso et al., 2012) and water retention constitutive models (Romero et al., 2011).

Microstructure of clays in reconstituted and compacted states has been assumed to be controlled by the conditions 'at formation' (Delage et al., 1983, Delage et al., 2006, Romero et al., 1999, Tarantino and Tombolato, 2005, Romero and Simms, 2008, Romero et al., 2011). Reconstituted clays typically show a mono-modal Pore-Size Distribution (PSD) with the dominant class of pores into the micro-pore range. Reconstituted clays are traditionally assumed to have a matrix-like fabric, with the mechanical behaviour controlled by particle-to-particle or cluster-to-cluster electro-chemical interactions (McConnachie, 1974). Sample compacted on the dry side of optimum (and at optimum water content) typically show a bi-modal PSD with two dominant classes of pores, one within the micro-pore range and the other within the macro-pore range (Delage et al., 1996, Tarantino and De Col, 2008). The bi-modal pore-size distribution is commonly associated with an aggregated microstructure with the macro-pores representing the intra-aggregate porosity and the micro-pores representing the inter-aggregate porosity respectively. On the other hand, clays compacted on the wet-side of optimum typically show a mono-modal pore-size distribution (Ahmed et al., 1974, Delage et al., 1996). These clays are generally assumed to have a microstructure similar to reconstituted clays because of the similar mono-modal PSD.

Although different compaction water contents give rise to different PSDs, Tarantino and De Col (2008) observed that the characteristic pore size associated with micro- and macro-porosities in compacted kaolin remain the same from very low water contents (dry-side of

optimum) up to the water content at optimum. As shown in Figure 1, kaolin sample compacted at optimum water content (w=0.311) shows a mono-modal PSD with modal size of ~0.2μm. Samples compacted at intermediate water contents on the dry side of optimum (w=0.141-0.259) show a micro-porosity in the same range (~0.2μm) in addition to a macro-porosity with modal size ~0.7 μm. At very low water content (w=0.086), the PSD becomes again mono-modal with the dominant size exactly in the same macro-porosity range (~0.7 μm).

The PSD of the sample compacted at very low water content (w=0.086) raises an apparent paradox with respect to the traditional view of compacted clay made of aggregates. This sample shows inter-aggregate porosity (macro-porosity) in the absence of intra-aggregate porosity (micro-porosity) and, hence, in the absence of aggregates!

Moreover, the (mono-modal) pore size distribution of reconstituted samples (Figure 1) is again characterised by the same micro-porosity range (~0.2μm) as shown by Tarantino (2010). In other words, the changes in PSD generated by different formation processes seem to be simply associated with a redistribution of pore volumes around the same two dominant pore-sizes. There is therefore a common thread across different microstructures generated within the same clay that have not yet been elucidated.

This paper aims to i) explore the continuity between the microstructure of reconstituted states (clay formed saturated) and compacted states (clay formed partially saturated) and ii) formulate a conceptual constitutive model unifying these states. The discussion is here limited to clays that are non-active.

One of the differences between reconstituted and compacted states (spanning from dry to wet of optimum) is represented by the nature and/or fraction of the pore-fluids at formation. Pores are either occupied by a single fluid (reconstituted soils) or by two fluids (compacted soils).

The strategy pursued to explore common features of these states was therefore to investigate the effect of various pore-fluids and their fractions. To this end, 'single-fluid' samples were prepared by saturating the pore space with fluids of different nature, i.e. water, acetone, and air. These samples will be referred to as water-saturated, acetone-saturated, and air-saturated samples. In addition, clay samples have been prepared by saturating the pore space with two fluids of different nature, air and water or air and acetone. These samples will be referred to as air/water-saturated and air/acetone-saturated samples.

MATERIAL AND SAMPLE PREPARATION

Speswhite kaolin with plastic limit $w_P=0.32$ and liquid limit $w_L=0.64$ was chosen for tests presented in this paper The grain size distribution showed it to have 0.20 silt fraction and 0.80 clay fraction.

Samples were prepared in five different ways for hydro-mechanical testing:

i)   Water-saturated samples were reconstituted from slurry by mixing dry powder of kaolin with demineralized water at water content equal to 0.96 (1.5 times the liquid limit);

ii)   Air-saturated samples were prepared from air-dried clay powder (at hygroscopic water content $w_h=0.006$). Preliminary tests showed that mechanical response of these samples under one-dimensional compression was not different from the samples prepared from clay powder oven-dried at 105 °C for 24h;

iii) Acetone-saturated samples were reconstituted from slurry by mixing dry clay powder with acetone. The samples were initially prepared to an acetone content equal to 0.96 (as the water-saturated samples);

iv)   Air/water saturated samples (compacted samples) were prepared by laying oven dried powder kaolin in a large plastic basin in layers of about 10 mm and spraying each layer with demineralised water to reach the target water content. The moistened powder was hand-mixed, and saturated lumps cut by means of a spatula. The sample was therefore tested without waiting for moisture equilibration. Preliminary tests showed that compaction behaviour and PSD of such samples were not different from samples tested after 24h moisture equilibration as per Tarantino and De Col (2008);

v)   Air/acetone saturated samples (sample compacted with acetone) were prepared according to the procedure described above, but acetone was used in place of water.

EXPERIMENTAL PROCEDURES

Single-fluid samples (air-, water-, and acetone- saturated) were subjected to 1-D mechanical compression in an oedometer cell (diameter 75 mm). Samples were loaded in steps (2, 3, 6, 12, 23, 45, 90, 178, 356, 711, 1422 kPa) to the target vertical stress (either 70kPa or 2220 kPa) and unloading was performed in one single step. Full consolidation was allowed for every loading/unloading step. Two-fluid samples (air/water- and air/acetone-saturated) were compacted statically in an oedometer cell (diameter 75 mm). The target vertical stress (either 300 or 1200 kPa) was reached in steps (150, 300, 600, 900, 1200 kPa). Although no drainage was allowed and proper sealing was made, the acetone content of the air/acetone saturated samples did not remain constant during static compaction because of the high volatility of acetone. In order to reduce the amount of evaporation of acetone,

the compaction tests took no more than 30 minutes. The acetone content was therefore measured at the end of the compaction test.

Finally, air/water saturated (compacted) samples and air-saturated samples were saturated with water in the oedometer cell by flooding the cell until the sample was submerged. Sample saturation was performed under various vertical stresses (nearly-zero vertical stress, 300 kPa and 1200kPa). After allowing for full consolidation, the saturated samples were then loaded in steps to the target vertical stress and unloaded in one single step.

Mercury intrusion porosimeter tests were carried out using an apparatus that measures pore entrance size in the range from 0.003 µm to 1000 µm as described in Pedrotti and Tarantino (2017). Samples prepared with water and subsequently tested in the MIP were dehydrated by means of the freeze-drying technique as described in Tarantino and De Col (2008) and Pedrotti and Tarantino (2017). Samples containing acetone were dehydrated by placing them in the oven (105 °C) for 24 hours. Because of the low surface tension of the acetone, sample disturbance due to oven-drying was assumed to be negligible. This was corroborated by the comparison of macroscopic void ratio with the void ratio extrapolated from MIP test.

EXPERIMENTAL RESULTS

Microstructure of samples saturated at formation with single-fluid or two-fluids

A water-saturated sample (reconstituted from slurry) and an air-saturated sample (formed from dry powder) were compressed to a vertical stress of 2220kPa and then unloaded. The PSD of these two samples is shown in Figure 2a. The same figure also reports the PSD of samples compacted to 1200 kPa at different water contents (from 0.09 to 0.32) according to Tarantino and De Col (2008). The compaction water

content and dry density of the samples whose PSD is shown in in Figure 2a are

illustrated in Figure 2b after Tarantino and De Col (2008).

The kaolin sample reconstituted from slurry (water-saturated) shows a mono-modal

pore size distribution with a modal value of ~0.2 μm. On the other hand, sample

compressed from dry powder (air-saturated) shows a modal value of ~0.60 μm.

The most striking aspect is that the PSD of the compacted air/water saturated

samples shows two modal sizes that essentially overlap with the modal size of the

water-saturated and air-saturated samples respectively. In addition, the void ratio

frequency redistributes as the water content changes and the air-saturated and

water-saturated samples appear to represent the two extremes of the redistribution

of frequencies in the compacted samples. The dominant pore size and the intrusion

volume frequency of the sample compressed from dry powder (air-saturated) are

higher than the ones of the sample reconstituted from slurry (water-saturated). This

is consistent with the higher repulsion Columbian forces between 'dry' particles in

turn associated with the lower dielectric permittivity of air (ε_{air}=1) compared to water

(ε_{water}=80) (Pedrotti and Tarantino, 2017).

The transition from dry to fully saturated microstructure is tentatively represented in

Figure 3. As the compaction water content increases (from right to left in Figure 3),

the volume of pores filled with air decreases and the volume of pores filled with water

increases.

The PSD of samples formed with single and two pore fluids were compared again in

an additional set of experiments where acetone was used in place of water. Figure

4a shows the PSD of air-saturated, acetone saturated, and air/acetone saturated

samples. The air/acetone saturated sample was compacted to 1200 kPa vertical

stress at nominal acetone content of 0.2 whereas the acetone-saturated sample

were consolidated from slurry to 2220 kPa. For purpose of comparison, the PSD of

the water-saturated sample is also reported in the Figure 4a. The compaction water

content and dry density of the samples whose PSD is shown in in Figure 4a are

illustrated in Figure 4b.

Figure 4a shows that the PSD of the acetone-saturated sample is mono-modal and this appear

to be a common feature of all single-fluid saturated samples (air, water, and acetone).

Furthermore, the PSD of the air/acetone-saturated sample is bi-modal and this appears to be a

common feature with the air/water-saturated sample.

Similarly to the case of air/water saturated samples (Figure 2) the two modal sizes of

the PSD of the compacted air/acetone saturated samples essentially overlap with the

modal size of the acetone-saturated and air-saturated samples respectively. It is also

worth noticing that the dominant size of the acetone-saturated pores is higher than

the one of the water saturated pores. Again, this is consistent higher repulsion

Columbian forces between particles in acetone due to the lower dielectric permittivity

of acetone ($\varepsilon_{acetone}$=24) compared to water (ε_{water}=80).

Regardless of the liquid (wetting fluid) used to prepare the sample by compaction,

the pore size of the micro-pores therefore appears to correspond to the dominant

pore size of the liquid-saturated sample (either acetone or water) whereas the modal

size of the macro-pores appears to correspond to the dominant pore size of the air-

saturated sample.

   As a result, for samples compacted with water, one can tentatively infer that

macro-pores are just pores filled with air (air-saturated) and micro-pores are just

pores filled with water (water-saturated). This is an unusual view of compacted soil

microstructure and is somehow in contrast with the traditional aggregate-based representation where micro-pores are associated with 'intra-aggregate' pores and macro-pores are associated with 'inter-aggregate pores' (Delage et al., 2006, Romero and Simms, 2008, Sivakumar et al., 2010, Tarantino, 2010, Monroy et al., 2010, Casini et al., 2012) as shown in Figure 5. To explore this assumption, additional experiments were carried out.

Microstructure evolution of compacted and dry samples upon saturation

The evolution of the PSD of three samples tested in the oedometer was examined (Figure 6):

i)   Sample 'formed unsaturated' - Compacted at w=0.12 to 1200 kPa, unloaded to 1 kPa and saturated;

ii) Sample 'formed dry' - Compressed from dry powder to 1200 kPa, unloaded to 1 kPa, and saturated;

iii) Sample 'formed saturated' - Reconstituted from slurry, consolidated to 70 kPa and unloaded to 1 kPa.

Figure 7 shows the pore-size distribution of kaolin sample compacted to 1200 kPa vertical stress before and after saturation under nearly zero vertical stress. Upon saturation the bi-modal PSD becomes mono-modal and this evolution of PSD can be interpreted as follows. The water-saturated pores (micro-pores) tend to rebound because pore-water pressure in these pores increases from negative values to zero. On the other hand, the initially air-saturated pores reduce their volume when they become saturated with water. The replacement of air with water causes a decrease in the Columbian repulsion forces between particles due to the higher dielectric permittivity of water, which in turn decreases the inter-particle distance. These two mechanisms are illustrated in Figure 8a and Figure 8b respectively.

Figure 9 shows the PSD of the sample compressed form dry powder before and after

saturation under nearly zero vertical stress. Before saturation the sample shows a mono-

modal PSD with the dominant porosity in the range of the macro-pores (~0.7μm). Upon

saturation, the PSD remains mono-modal but the dominant porosity switches to the range of

micro-pores (~0.2μm). In this case, only the mechanism depicted in Figure 8b takes place

upon saturation. As a result, samples prepared from dry powder experience volumetric

collapse upon saturation even at very low vertical stress as shown in Figure 6.

Figure 10 shows the PSDs of the samples formed under dry and unsaturated (compacted)

conditions and then saturated. These are compared with the PSD of the sample formed

saturated (reconstituted). The PSDs are very similar and different conditions 'at formation'

do not appear to generate samples that are microstructurally different as often assumed in the

literature. Figure 10 also shows once again that the 'dry' state is one of the extremes of the

possible states of a clay.

Continuity of macroscopic behaviour across different states

Figure 11a shows two samples compacted in an oedometer cell to 300 and 1200 kPa

respectively at water content w=0.12. After compaction (point 1), the samples were unloaded

to 1 kPa (point 2), saturated (point 3), and then loaded to 2220 kPa (point 4). The void ratio

change associated with this hydro-mechanical paths is shown in Figure 11a together with the

compression curve of the reconstituted clay (formed water-saturated) and dry clay (formed

air-saturated).

At the end of compaction (point 1), the two samples lie between the air-saturated and water-

saturated normal compression curves. The sample having the higher degree of saturation at

compaction, i.e. the sample compacted to 1200 kPa, appears to be closer to the normal

consolidation line of the water-saturated (reconstituted from slurry) sample. Upon saturation,

the void ratio of the two samples increased (path 2-3). The higher the degree of saturation

after unloading (point 2), the higher was the amount of void ratio increase (swelling)

occurring upon saturation (path 2-3), i.e. the sample compacted to 1200 kPa, exhibited higher

swelling. Finally, following saturation, the saturated compression curves of the two

compacted samples appear to join the normal consolidation line of the sample reconstituted

from slurry, after having initially exhibited an over-consolidation-like response upon loading.

Figure 11b shows a sample compacted to 1200 kPa (point 1), saturated under 1200 kPa

vertical stress (point 2), unloaded to 1 kPa (point 3), and finally re-loaded to 2220 kPa.

Following saturation, the sample collapses on the normal consolidation line of the

reconstituted sample. The re-loading curve joins again the normal consolidation line of the

reconstituted sample.

The fact that compacted samples tend to join the same normal compression line after

saturation, regardless of whether saturation is attained at high or very low vertical stress, is

not a new finding. However, the striking aspect in Figure 11 is that the normal compression

line attained by the compacted samples after saturation coincides with the normal

compression of samples reconstituted from slurry. This highlights the continuity between

compacted and reconstituted states

The mechanical response of samples prepared from dry powder (born air-saturated) and

subjected to saturation is illustrated in Figure 12. Tests were similar to the ones presented in

Figure 11 with the only difference that only one fluid was initially filling the pores, i.e. air, in

contrast to the compacted samples where two fluids were present in the pores at formation,

i.e. air and water.

Figure 12a shows two air-saturated samples (prepared from dry powder) saturated at nearly

zero vertical stress. One sample was subjected to 1kPa (point 1), saturated (point 3), and then

loaded to 2220 kPa (point 4). A second sample was compressed to 300 kPa (point 1'),

unloaded to 1 kPa (point 2'), saturated (point 3'), and then loaded to 2220 kPa (point 4 in

Figure 12a). Figure 12a also shows the compression curves of the water-saturated

(reconstituted from slurry) and air-saturated samples (dry powder) for purpose of comparison.

Upon saturation at quasi-zero vertical stress, the air-saturated samples exhibited a volumetric

collapse in contrast to the swelling that would have been exhibited by a compacted sample.

Upon loading, both samples join the normal consolidation line of the sample reconstituted

from slurry (path 3-4), in a way very similar to the compacted samples shown in Figure 11a.

This highlights again the continuity between dry and reconstituted states and the fact that

these two states 'bound' the compacted states.

Figure 12b shows a sample compressed dry to 300 kPa (point 1 in Figure 12b), saturated

under 300 kPa vertical stress (point 2 in Figure 12b), unloaded to 1 kPa (point 3 in Figure

12b) and re-loaded to 2220 kPa (point 4 in Figure 12b). Upon saturation, this sample also

showed a volumetric collapse moving from the air-saturated (dry powder) normal

consolidation line to the water-saturated (reconstituted from slurry) normal compression line.

The response of dry clay upon saturation differs from the compacted clay where micro-pores

swell and macro-pores collapse as shown in Figure 8. In compacted samples, these two

competing mechanisms cause the compacted sample to experience either swelling under low

vertical stress or volumetric collapse at high vertical stress upon saturation (Figure 11b).

It is worth observing that the concomitance of swelling and collapse mechanisms in

compacted soils upon saturation is also returned by the aggregate-based microstructural

model. Collapse of the macro-pores is associated with slippage at aggregate contacts whereas

swelling of micro-pores is associated with the swelling of the aggregates themselves. What

the aggregate-based microstructural model cannot justify is the collapse experienced by

samples prepared from dry powder regardless of the stress level, which can be indeed

inferred from the particle-based microstructural model put forward in Figure 5 and Figure 8.

CONCEPTUAL CONSTITUTIVE MODEL FOR NON-ACTIVE CLAY

The microstructural investigation presented above led to the assumption that unsaturated

(compacted) clay is made of air-saturated and water-saturated pores. A second assumption is

made in this paper, i.e. the air-saturated part behaves as the air-saturated clay (compressed

from dry powder) and the water-saturated part behaves as the water-saturated clay

(reconstituted from slurry). A conceptual constitutive model is built around these two

assumptions in the following sections and validated against different hydro-mechanical paths

under 1-D conditions.

Void ratio

Let us define the void ratio of the air-saturated fraction, e^A, and the void ratio of the water-

saturated fraction, e^W, as follows:

$$e^A = \frac{V_V^A}{V_S^A} \; ; \; e^W = \frac{V_V^W}{V_S^w} \tag{1}$$

where V_V^A = volume of air-saturated voids, V_S^A = volume of solids surrounded by air, V_V^W =

volume of water-saturated voids, and V_S^w = volume of solids surrounded by water.

If the volume of voids of an air-water saturated sample, V_V , is considered to be the sum of

the volume of air-saturated voids , V_V^A, and the volume of water-saturated voids, V_V^W:

$$V_V = V_V^W + V_V^A \tag{2}$$

the following equation can be derived for the total void ratio (see Appendix for full

derivation):

$$e = \frac{e^W \cdot e^A}{e^W \cdot (1 - S_R) + e^A \cdot S_R} \tag{3}$$

where S_R is the degree of saturation (ratio between the volume of water saturated voids, V_V^W,

and the total volume of voids, V_v).

The void ratio e can therefore be derived from the void ratios e^A and e^W, which can be in turn

read on the compression curves of the air-saturated and water-saturated clay as illustrated in

Figure 13. To this end, the effective stresses acting on the air-saturated and the water-

saturated part need to be identified.

Effective stresses

Bishop (1960) derived the effective stress for saturated media by assuming that

i)   'Only the part of the local contact stress which is in excess of the fluid pressure causes

        deformation of the soil structure'

ii)   The intergranular stress is derived by considering the equilibrium of forces across a

        wavy plane passing through points of inter-particle contacts.

Similarly to the case of a saturated sample, it was assumed that the effective stress for

partially saturated soils σ' is still derived from the 'deviatoric' forces acting on the particles.

This leads to the following expression (see Appendix for full derivation):

$$\sigma' = \sigma'_W + \sigma'_A = (\sigma - u_w)S_R + (\sigma - u_A)(1 - S_R) \qquad [4]$$

The assumption made in this work is that the first term on the right-hand side of Equation [4]

controls the response of the water-saturated part (whereas the second term on the right-hand

side of Equation [4] controls the response of the air-saturated part. Therefore, the effective

stresses acting on the water-saturated part, σ'_W, and the air-saturated part, σ'_A, are postulated as

follows:

$$\sigma'_W = (\sigma - u_w) \cdot S_r \tag{5}$$

$$\sigma'_A = (\sigma - u_A) \cdot (1 - S_r) \tag{6}$$

Mechanical response of pores with no fluid transition

For a given hydro-mechanical path, each pore will behave according to its pore fluid, which determines its effective stress and its compressibility. Water-saturated pores will compress/rebound as in samples reconstituted from slurry. Whether water-saturated pores are moving along the normal consolidation line (*ncl*) or the unloading-reloading line (*url*), this depends on the pre-consolidation void ratio, intended here as the minimum void ratio that water saturated pores have ever experienced. For example, Figure 14a shows the path of water-saturated pores initially normally consolidated subjected to either loading or unloading respectively. The changes in void ratio of the water-saturated fraction are given as follows:

$$(\Delta e^{WW})_{ncl} = -\lambda_w \, \Delta(ln\sigma'_w)$$
$$(\Delta e^{WW})_{url} = -k_w \, \Delta(ln\sigma'_w) \tag{7}$$

where λ_w and κ_w are the slopes of the *ncl* and the *url* for the clay reconstituted from slurry respectively. The subscript *WW* indicates pores that are water-saturated before and after the change in effective stress σ'_w.

Similarly, air-saturated pores will compress/rebound as in samples prepared from dry powder. The changes in void ratio of the air-saturated fraction are given as follows:

$$(\Delta e^{AA})_{ncl} = -\lambda_A \, \Delta(ln\sigma'_A)$$
$$(\Delta e^{AA})_{url} = -k_A \, \Delta(ln\sigma'_A) \tag{8}$$

where λ_A and κ_A are the slopes of the *ncl* and the *url* for the clay prepared from dry powder respectively (Figure 14b). The subscript *AA* indicates the pores that are air-saturated before and after the change in effective stress σ'_A.

Mechanical response of pores with fluid transition

The effect of an increase in degree of saturation (wetting) is shown in Figure 15a. Water-saturated pores do not change their state and remain water-saturated (such pores are denoted with e^{WW} since they move from a water-saturated state –W- to another water-saturated state –W). On the other hand, air-saturated pores split in two different sub-classes upon wetting. One fraction of these pores remains air-saturated (such pores are denoted with e^{AA} since they move from an air-saturated state –A- to another air-saturated state –A). A second fraction of air-saturated pores becomes water-saturated (such pores are denoted with e^{AW} since they move from an air-saturated state –A- to a water saturated state –W).

The path of the water-saturated and air-saturated pores is the one shown in Figure 14 for the case of pores with no fluid transition. An example of the path of the pores that are initially air-saturated and becomes water-saturated (fluid transition) upon a wetting path is shown in Figure 16. These pores initially lie on the air-saturated ncl and then move to the water-saturated ncl.

To compute the change in void ratio Δe^{AW}, it is convenient to introduce an equivalent water-saturated pre-consolidation stress $\sigma'_W{}^*$. As shown in Figure 16, this is given by the water-saturated effective stress that returns a void ratio on the water-saturated ncl equal to the void ratio before the change of state.

Accordingly, the change in void ratio Δe^{AW} is given by:

$$(\Delta e^{AW}) = -\lambda_w \ln\left(\frac{\sigma'_w}{\sigma'_w{}^*}\right) \qquad [9]$$

For the case shown in Figure 16, the equivalent water-saturated pre-consolidation stress $\sigma'_W{}^*$ is exceeded by the current water-saturated effective stress σ'_w and the 'equivalent' water-saturated path occurs along the ncl, i.e. plastic deformations take place. In other words, this class of pores experience volumetric collapse upon wetting.

Figure 15b shows the effect of a decrease in degree of saturation (drying). The air-saturated pores do not change their state and remain air-saturated (such pores are denoted with e^{AA} since they move from an air-saturated state –A- to another air-saturated state –A). On the other hand, water-saturated pores split in two different sub-classes upon drying. One fraction of these pores remains water-saturated (such pores are denoted with e^{WW} since they move from a water-saturated state –W- to another water-saturated state –W). A second fraction of water-saturated pores becomes air-saturated (such pores are denoted with e^{WA} since they move from a water-saturated state –W- to an air-saturated state –A).

An example of the path of the pores that are initially water-saturated and becomes air-saturated upon a drying path is shown in Figure 17. These pores lie initially on the water-saturated ncl and then move to an air-saturated url.

To compute the change in void ratio Δe^{WA}, it is convenient to introduce an equivalent air-saturated pre-consolidation stress $\sigma'_A{}^*$. As shown in Figure 17, this is given by the air-saturated effective stress that returns a void ratio on the air-saturated ncl equal to the void ratio before the change of state.

For the case shown in Figure 16, the equivalent air-saturated pre-consolidation stress $\sigma'_A{}^*$ is

not exceeded by the current air-saturated effective stress σ'_A and the 'equivalent' air-

saturated path occurs along the url,

Accordingly, the change in void ratio Δe^{WA} is given by:

$$(\Delta e^{WA}) = -k_A \ln\left(\frac{\sigma'_A}{\sigma'_A{}^*}\right)$$

[10]

SIMULATION OF HYDRO-MECHANICAL PATHS OF UNSATURARED SAMPLES

Simulation of loading and unloading at constant water content (compaction)

The experimental data presented by Tarantino and De Col (2008) were considered

for the simulation. Six samples were loaded and unloaded at constant water content

to 300, 600, 900 and 1200 kPa respectively with water content ranging from w=0.236

to w=0.311. Compression at constant water content (compaction) was carried out in

a modified oedometer cell where suction was measured by high-capacity

tensiometers during the compaction process. As an example, Figure 18 shows the

results of the test on the specimen at w=0.254 in terms of void ratio versus total

stress and degree of saturation versus matric suction.

Because the test involves both loading (e.g. 4 to 5) and unloading paths (e.g. 5 to 6),

these are discussed separately.

Mechanical loading path

Upon loading, the void ratio decreases at constant water content. The hydraulic path is

therefore a wetting path since the degree of saturation increases. Accordingly, the pores

follow the pattern shown in Figure 15a.

The water-saturated pores and the air-saturated pores that do not change their state move along the water-saturated ncl (Δe^{WW}) and the air-saturated ncl respectively (Δe^{AA}) (Figure 19). The air-saturated pores that become water-saturated move from the air-saturated ncl to the water-saturated ncl (Δe^{AW} in Figure 19). These pores therefore experience volumetric collapse as discussed in Figure 16.

The wetting path generates a new fraction of water-saturated pores that experience a void ratio change (Δe^{AW}) that adds to the fraction of pores that were already saturated and are subjected to the change Δe^{WW}. To compute the overall change in water-saturated void ratio Δe^{W}, the volume of solids of these two fractions need to be considered. If V_s^{WW} is the volume of solids of the fraction that remains water-saturated and V_s^{AW} is the volume of solids of the fraction that becomes water-saturated, the total volume of 'wet' solids is given by $V_s^{W} = V_s^{AW} + V_s^{WW}$.

The water-saturated void ratio Δe^{W} is therefore given by a weighted average of the two water-saturated void ratio changes:

$$\Delta e^W = \Delta e^{WW} \cdot \left(1 - \frac{V_s^{AW}}{V_s^{W}}\right) + \Delta e^{AW} \frac{V_s^{AW}}{V_s^{W}} \qquad [11]$$

The volume of the solids V_s^{AW}, i.e. the volume of the solids that becomes wetted upon an increase in degree of saturation (wetting) can be reasonably assumed to be proportional to the increase in degree of saturation ΔS_r. Accordingly, the most convenient assumption for the ratio V_s^{AW}/V_s^{W} is:

$$\frac{V_s^{AW}}{V_s^{W}} = \frac{\Delta S_r}{S_r}$$

Eq. [11] therefore becomes:

$$\Delta e^W = \Delta e^{WW} \cdot \left(1 - \frac{\Delta S_r}{S_r}\right) + \Delta e^{AW} \frac{\Delta S_r}{S_r} \qquad [12]$$

Mechanical unloading path

Upon unloading, the void ratio decreases at constant water content. The hydraulic path is

therefore a drying path since the degree of saturation decreases. Accordingly, the pores

follow the pattern shown in Figure 20a. The air-saturated pores and the water-saturated pores

that do not change their state move along the water-saturated url (Δe^{WW}) and the air-saturated

url respectively (Δe^{AA}) and experience rebound (Figure 19). The water-saturated pores that

become air-saturated move from the water-saturated ncl to the air-saturated url (Δe^{WA} in

Figure 17 and Figure 20a). These pores also experience volumetric rebound.

The drying path generates a new fraction of air-saturated pores that experience a

void ratio change (Δe^{WA}) that adds to the fraction of pores that were and remain air-

saturated and are subjected to the void ratio change Δe^{AA}. To compute the overall

change in air-saturated void ratio Δe^A, the volume of solids of these two fractions

needs to be considered.

The air-saturated void ratio Δe^A is given by a weighted average of the two air-

saturated void ratio changes. With similar arguments as above, one can write:

$$\Delta e^A = \Delta e^{AA} \cdot \left[1 - \frac{(-\Delta S_r)}{1 - S_r}\right] + \Delta e^{AW} \frac{(-\Delta S_r)}{1 - S_r} \qquad [13]$$

Test simulation

To simulate the loading and unloading paths of the type shown in Figure 18:

i) The applied vertical stress, the suction, and the degree of saturation measured during the test were taken as input data (Tarantino and De Col, 2008)

ii) The compressibility indexes of kaolin reconstituted from slurry and kaolin prepared from dry powder taken as the only 'constitutive' parameters.

iii) The initial states of the air-saturated and water-saturated fractions are both normally consolidated.

The compressibility indexes assumed for the water-saturated and air-saturated pores are shown in Figure 21 (the experimental curves are also shown for reference)

Figure 22 shows the simulated paths for the loading and unloading at constant water content together with the experimental data. The simulation shows an excellent agreement with the experimental data. This is a remarkable achievement considering that no fittings parameters have been used and only the compression curves for water-saturated clay (reconstituted from slurry) and air-saturated clay (prepared from dry powder) were used to model the experimental data.

To better highlight the separate compression of air-saturated and water-saturated pores, Figure 23 shows the compression paths of the water-saturated part, e^W, and the compression path of the air-saturated part, e^A, for the sample compacted at w=0.236. For the virgin compression, the paths followed by the water saturated and air-saturated pores both lie on their relative ncl. At any step, the void ratio of the compacted sample is the weighted average of the air-saturated and water-saturated pores, i.e. the compression curve of the unsaturated (compacted) sample lies between ncl of the clay reconstituted from slurry and the clay prepared from dry powder respectively. Furthermore, since the degree of saturation increases

upon loading, the compaction curve tends to converge to the water-saturated ncl

(reconstituted from slurry).

Simulation of saturation (hydraulic wetting) and subsequent mechanical loading

A test involving saturation of a compacted sample was considered to test the conceptual

constitutive model. The test was characterised by three steps as shown in Figure 24:

- Step 0-1-2: compaction at constant water content (w=0.12) to 1200 kPa vertical stress and

subsequent unloading to 1kPa. State 2 is the state commonly referred to 'as-compacted' state.

- Step 2-3: saturation under quasi-zero vertical stress

- Step 3-4: reloading under saturated conditions

The approach followed to simulate the path 0-1-2 is the one illustrated the previous section.

The focus here is the simulation of the swelling upon saturation (path 2-3) and the following

reloading under saturated conditions (path 3-4).

The path followed by the pores in step 2-3 is shown Figure 25a. At point 2, air-

saturated and water-saturated pores are both present. The sample is subjected to

quasi-zero total stress and only the suction contributes to the water-saturated

effective stress. Upon saturation, the water-saturated pores that were and remain

saturated experience swelling due to the decrease in suction (Δe^{WW} in Figure 25a).

On the other hand, the air-saturated pores become water-saturated. As discussed in

Figure 16, such pores experience volumetric collapse as they move to the water-

saturated *ncl* (Δe^{AW} in Figure 25a). The total change in void ratio experienced upon

saturation depends on the competition between these two mechanisms. As shown in

the simulation in Figure 24, the swelling mechanism was found to prevail in this

specific case.

The path 3-4 only involves water-saturated pores. However, two fractions needs to be considered, the pores the experienced the void ratio changes Δe^{WW} and Δe^{AW} respectively. Although these two fractions are both subjected to the same water-saturated effective stress, their history is different in the sense that they are characterised by a different pre-consolidation stress, i.e. one fraction lies on the *url* (WW) and one fraction lies on the *ncl* (AW). These fractions therefore experience different void ratio change when the effective stress is increased (Figure 25b). The overall void ratio therefore moves between the *ncl* and the *url* of the reconstituted sample as shown in Figure 25b until a virgin state is attained by the class of pores initially over-consolidated.

The simulation of the paths 0-1-2, 2-3 and 3-4 is shown in Figure 24. For the first path, suction and degree of saturation was inferred from a test reported in Tarantino and De Col (2008) carried out at same water content and maximum vertical stress. The quality of the simulation of this path is in line with the simulation of the loading-unloading path shown in the previous section.

Simulation of the paths 2-3 and 3-4 appears to capture quite well the swelling upon saturation and the subsequent reloading. Again, the accuracy of this simulation is remarkable if one considers that the mechanical constitutive parameters were only derived from the compression curves of the clay reconstituted from slurry and compressed from dry powder.

Simulation of volume change of reconstituted kaolin upon drying

A test presented by Tarantino (2010) was used for this simulation. Kaolin clay was consolidated from slurry to 100 kPa vertical stress, removed from the oedometer, and then let dry to different target water contents. Figure 26 shows the evolution of the degree of

saturation and the void ratio as suction increases upon drying. Under saturated conditions, the specimen follows the ncl. Beyond the air-entry suction, the specimen shows a tendency to rebound.

The path followed by the pores in the saturated range is trivial. This specimen was reconstituted from slurry and therefore all the pores initially follow the water-saturated ncl. Beyond the air entry suction, two classes of pores are present, the water-saturated pores that remain water-saturated (WW) and the air-saturated pores that were previously water-saturated (AW).

Pores that remain water-saturated move along the water saturated ncl and experience a decrease in void ratio Δe^{WW}. Pores that become air-saturated moves to an air-saturated url and experience a rebound Δe^{WA} as shown in Figure 27. The overall void ratio change depends on the competition between these two opposite mechanisms.

The simulation of this test is shown in Figure 26. Suction and degree of saturation were taken from the experimental data and used as input variables. The ncl of the water saturated kaolin (reconstituted from slurry) was used as reference for the water-saturated part and the air-saturated url (dry powder) as reference for the drying process. The simulation captures quite well the response of the clay in the unsaturated range. In this specific case, the rebound of the pores that dry out prevail on the shrinkage of the pores that remain saturated and the overall void ratio increases upon drying.

CONCLUSIONS

This paper has presented an experimental investigation aimed at exploring the continuity between the microstructure of reconstituted and compacted states. The pore-size distribution (PSD) of compacted samples has been compared with the PSDs of samples reconstituted from slurry and samples prepared from dry powder respectively.

Compacted samples show a bi-modal pore-size frequency distribution characterised by

micro-pores and macro-pores. It has been shown that the distribution of the micro-pores is

associated with the distribution of pores in samples reconstituted from slurry and the

distribution of the macro-pores is associated with the distribution of pores in sample prepared

from dry powder. This has led to a different view of compacted soil microstructure where

macro-pores are assumed to be just pores filled with air (air-saturated) and micro-pores are

assumed to be just pores filled with water (water-saturated).

The evolution of PSD has then been inspected upon saturation paths under quasi-zero stress

involving unsaturated (compacted) and dry (compressed from dry powder) samples. It has

been shown that the PSD of samples in saturated state (at given vertical stress) is the same

irrespective of whether the sample was formed saturated (reconstituted from slurry),

unsaturated (compacted), or dry (from clay powder). This appears to support the idea that

there are two classes of pores in clay, one filled with water (water-saturated) and the other

one filled with air (air-saturated).

Based on this idea, a conceptual constitutive model has been formulated based on two core

assumptions, i) unsaturated (compacted) clay is made of air-saturated and water-saturated

pores, and ii) the air-saturated part behaves as the air-saturated (compressed from dry

powder) clay and the water-saturated part behaves as the water-saturated (reconstituted from

slurry) clay.

After identifying the 'effective' stresses acting on the dry and saturated part of the

clay, complex hydro mechanical paths have been modelled, including loading and

unloading at constant water content, saturation of an initially unsaturated

(compacted) clay, and drying of an initially saturated (reconstituted from slurry) clay.

The simulations captured quite well the experimental data. It is remarkable that

simulations were based on constitutive parameters derived only from the

compression behaviour of clay under dry (formed from dry powder) and saturated

(reconstituted from slurry) conditions.

APPENDIX

Void ratio

The volume of voids, V_V , in an unsaturated sample is equal to the sum of the volume of air-saturated voids, V_V^A, and the volume of water-saturated voids, V_V^W:

$$V_V = V_V^W + V_V^A \qquad [14]$$

The void ratio of an unsaturated sample, e is defined as the ratio between the volume of voids V_V and the volume of solids, V_s . By dividing both members of Equation [14] by V_s the following Equation [15] is obtained:

$$e = \frac{V_V}{V_S} = \frac{V_V^W}{V_S} + \frac{V_V^A}{V_S} \qquad [15]$$

Let us multiply and divide the term V_V^W by the volume of solids of the wet particles, V_S^W, and multiply and divide the term V_V^A by the volume of solids of the dry particles, V_S^A. The void ratio of the compacted soil, e can be expressed as follows:

$$e = \frac{V_V^W}{V_S^W} \cdot \frac{V_S^W}{V_S} + \frac{V_V^A}{V_S^A} \cdot \frac{V_S^A}{V_S} \qquad [16]$$

The void ratio of the saturated part, e^W, is defined as $\frac{V_V^W}{V_S^W}$ and the void ratio of the dry part, e^A, is defined as $\frac{V_V^A}{V_S^A}$. Moreover, the volume of solids of the dry particles, V_S^A, may be expressed as the difference between the volume of solids of the whole compacted sample, V_s and the volume of solids of the wet particles, V_S^W. Equation [16] can then be re-written as:

$$e = e^W \cdot \frac{V_S^W}{V_S} + e^A \cdot \left(1 - \frac{V_S^W}{V_S}\right) \qquad [17]$$

The degree of saturation, S_R, is defined as the ratio $\frac{V_V^W}{V_V}$. By multiplying and dividing such

ratio by the volume of solids of the compacted sample, V_S and by re-arranging, the following

expression for the degree of saturation is obtained:

$$S_R = \frac{V_V^W}{V_V} = \frac{V_V^W}{V_S} \cdot \frac{V_S}{V_V} = \frac{V_V^W}{V_S} \cdot \frac{1}{e} \qquad [18]$$

In the same way, if the second member of equation [18] is multiplied and divided by the

volume of solids of the wet particles, V_s^W, Equation [19] is obtained

$$S_R = \frac{V_V^W}{V_S} \cdot \frac{1}{e} = \frac{V_V^W}{V_S^W} \cdot \frac{V_S^W}{V_S} \cdot \frac{1}{e} = \frac{V_S^W}{V_S} \cdot \frac{e^W}{e} \qquad [19]$$

If the term $\frac{V_S^W}{V_S}$ is isolated from Equation [19] as follows:

$$\frac{V_S^W}{V_S} = S_R \cdot \frac{e}{e^W} \qquad [20]$$

and substituted into Equation [17], the relationship of the void ratio of the unsaturated

samples, e, as a function of the void ratio of the wet particles, e^W, the void ratio of the dry

particles, e^A, and the degree of saturation, S_R, is finally derived:

$$e = \frac{e^W \cdot e^A}{e^W \cdot (1 - S_R) + e^A \cdot S_R} \qquad [21]$$

Effective stresses

Effective stress for partially saturated soils σ' is derived from the 'deviatoric' forces acting on

the particles

$$\sigma' A = \sum P_i^W - u_w \sum A_{si}^W + \sum P_i^A - u_A \sum A_{si}^A \qquad [22]$$

where P_i^W and P_i^A are the forces at each contact for particles water-saturated and air-saturated respectively, A is the unit area of the plane, A_{si}^W and A_{si}^A are the contact area for water- and air-saturated particles respectively, u_w is the water pore pressure, and u_A is the air pore pressure.

By considering the equilibrium across the wavy plane as shown in Figure 28b and by defining σ_i as the average intergranular force per unit area of the plane, A, we have:

$$\sigma_i \ = \frac{\sum P_i^W + \sum P_i^A}{A} = \sigma - u_w \frac{(A^W - \sum A_{si}^w)}{A} - u_A \frac{(A^A - \sum A_{si}^A)}{A} \qquad [23]$$

where A^W and A^A are the area of the plane water-saturated and air-saturated respectively

By combining equation [22] and [23] and by splitting the external stress σ between the water-saturated area, A^W, and the air-saturated area, A^A:

$$\sigma' = (\sigma - u_w)\left(\frac{A^W}{A}\right) + (\sigma - u_A)\left(1 - \frac{A^W}{A}\right) \qquad [24]$$

By assuming that $\frac{A^W}{A}$ equals the degree of saturation, S_R, Equation [24] can be re-written as follows:

$$\sigma' = \sigma'_W + \sigma'_A = (\sigma - u_w)S_R + (\sigma - u_A)(1 - S_R) \qquad [25]$$

References

AHMED, S., LOVELL, C. & DIAMOND, S. Pore sizes and strength of compacted clay: 14F, 2T, 15R. J. GEOTECH. ENGNG. DIV. V100, N. GT4, APR. 1974, P407–425. International Journal of Rock Mechanics and Mining Sciences & Geomechanics Abstracts, 1974. Pergamon, A161.

ALONSO, E., PINYOL, N. & GENS, A. 2012. Compacted soil behaviour: initial state, structure and constitutive modelling. Geotechnique, 63, 463-478.

BISHOP, A. W. 1960. The principles of effective stress, Norges Geotekniske Institutt.

CASINI, F., VAUNAT, J., ROMERO, E. & DESIDERI, A. 2012. Consequences on water retention properties of double-porosity features in a compacted silt. Acta Geotechnica, 7, 139-150.

DELAGE, P., AUDIGUIER, M., CUI, Y.-J. & HOWAT, M. D. 1996. Microstructure of a compacted silt. Canadian Geotechnical Journal, 33, 150-158.

DELAGE, P., LEFEBVRE, G., SRIDHARAN, A., JAYADEVA, M., MURTY, B. & NAGARAJ, T. 1983. Double-layer theory and compressibility of calys-discussion. Thomas Telford Services LTD. Thomas Teldford House, 1 Heron Quay, London England E14 4JD.

DELAGE, P., MARCIAL, D., CUI, Y. & RUIZ, X. 2006. Ageing effects in a compacted bentonite: a microstructure approach. Geotechnique, 56, 291-304.

GALLIPOLI, D., GENS, A., SHARMA, R. & VAUNAT, J. 2003. An elasto-plastic model for unsaturated soil incorporating the effects of suction and degree of saturation on mechanical behaviour. Géotechnique., 53, 123-136.

MCCONNACHIE, I. 1974. Fabric changes in consolidated kaolin. Geotechnique, 24, 207-222.

MONROY, R., ZDRAVKOVIC, L. & RIDLEY, A. 2010. Evolution of microstructure in compacted London Clay during wetting and loading. Geotechnique, 60, 105-119.

PEDROTTI, M. & TARANTINO, A. 2017. An experimental investigation into the micromechanics of non-active clays. Géotechnique, 1-18.

ROMERO, E., DELLA VECCHIA, G. & JOMMI, C. 2011. An insight into the water retention properties of compacted clayey soils. Geotechnique, 61, 313.

ROMERO, E., GENS, A. & LLORET, A. 1999. Water permeability, water retention and microstructure of unsaturated compacted Boom clay. Engineering Geology, 54, 117-127.

ROMERO, E. & SIMMS, P. H. 2008. Microstructure investigation in unsaturated soils: a review with special attention to contribution of mercury intrusion porosimetry and environmental scanning electron microscopy. Geotechnical and Geological Engineering, 26, 705-727.

SIVAKUMAR, V., SIVAKUMAR, R., MURRAY, E., MACKINNON, P. & BOYD, J. 2010. Mechanical behaviour of unsaturated kaolin (with isotropic and anisotropic stress history). Part 1: wetting and compression behaviour. Géotechnique, 60, 581-594.

TARANTINO, A. 2007. A possible critical state framework for unsaturated compacted soils. Geotechnique, 57, 385-389.

TARANTINO, A. Unsaturated soils: compacted versus reconstituted states. 5th International Conference on Unsaturated Soil, 2010. 113-136.

TARANTINO, A. & DE COL, E. 2008. Compaction behaviour of clay. Geotechnique, 58, 199-213.

TARANTINO, A. & TOMBOLATO, S. 2005. Coupling of hydraulic and mechanical behaviour in unsaturated compacted clay. Geotechnique, 55, 307-317.
WHEELER, S., SHARMA, R. & BUISSON, M. 2003. Coupling of hydraulic hysteresis and stress–strain behaviour in unsaturated soils. Geotechnique, 53, 41-54.

LIST OF CAPTIONS FOR ILLUSTRATIONS

Figure 1. PSD of samples compacted at the same vertical stress but different water content and PSD of sample reconstituted from slurry (modified from Tarantino (2010).

Figure 2. (a) PSDs of air/water saturated (compacted) samples, water-saturated (reconstituted) samples, and air-saturated (compressed from dry powder) samples. (b) Dry density and water content of compacted samples tested for MIP.

Figure 3. Schematic representation of different conditions "at formation" (samples reconstituted from slurry, compacted at target water content, and compressed from dry powder).

Figure 4. (a) Pore size distribution of water-saturated, acetone-saturated, air/acetone saturated, and air-saturated kaolin samples. (b) Dry density and water content of air/acetone saturated (compacted) sample tested for MIP.

Figure 5. Comparison between traditional "aggregate-based" and "pore-fluid-based" microstructure model.

Figure 6. Hydro-mechanical paths followed by samples i) formed dry (compressed from dry powder) and then saturated, ii) formed unsaturated (compacted) and then saturated, and iii) formed saturated (reconstituted).

Figure 7. PSDs of kaolin sample compacted to 1200 kPa vertical stress before and after saturation under nearly zero vertical stress.

Figure 8. Pore mechanical response upon saturation (a) Micro-pore swelling and (b) macro-pore collapse.

Figure 9. PSDs of samples prepared from dry powder before and after saturation under quasi-zero vertical stress.

Figure 10. PSDs of samples having similar void ratio under saturated conditions but formed under dry, unsaturated (compacted), or saturated (reconstituted) conditions.

Figure 11. (a) Kaolin samples compacted to 300 and 1200 kPa vertical stress, unloaded, and saturated under near-zero vertical stress (b) Kaolin samples compacted to 1200 kPa vertical stress and saturated under 1200 kPa vertical stress.

Figure 12. (a) Kaolin samples prepared from dry powder saturated at nearly-zero vertical stress (b) Kaolin sample prepared from dry powder, compressed to 300 kPa vertical stress, and saturated under 300 kPa vertical stress.

Figure 13. Constitutive modelling framework

Figure 14. Mechanical path for (a) water-saturated pores e^{WW} and (b) air-saturated pores e^{AA},

Figure 15. Change in degree of saturation upon (a) wetting paths and (b) drying paths.

Figure 16. Mechanical path for air-saturated pores that boecme water-saturated e^{AW}

Figure 17. Mechanical path for water-saturated pores that become air-saturated e^{WA}

Figure 18. Compaction test for specimen having w=0. 254. (a) Void ratio versus vertical stress. (b) Degree of saturation versus matric suction (Tarantino and De Col, 2008).

Figure 19. Pore response upon mechanical loading at constant water content of a compacted sample.

Figure 20. Pore response upon mechanical unloading at constant water content of a compacted sample.

Figure 21. 'Constitutive' compression curves derived from (a) reconstituted (formed water-saturated) samples and (b) dry (formed from dry powder) samples.

PedrottiFigure01

PedrottiFigure02a

PedrottiFigure02b
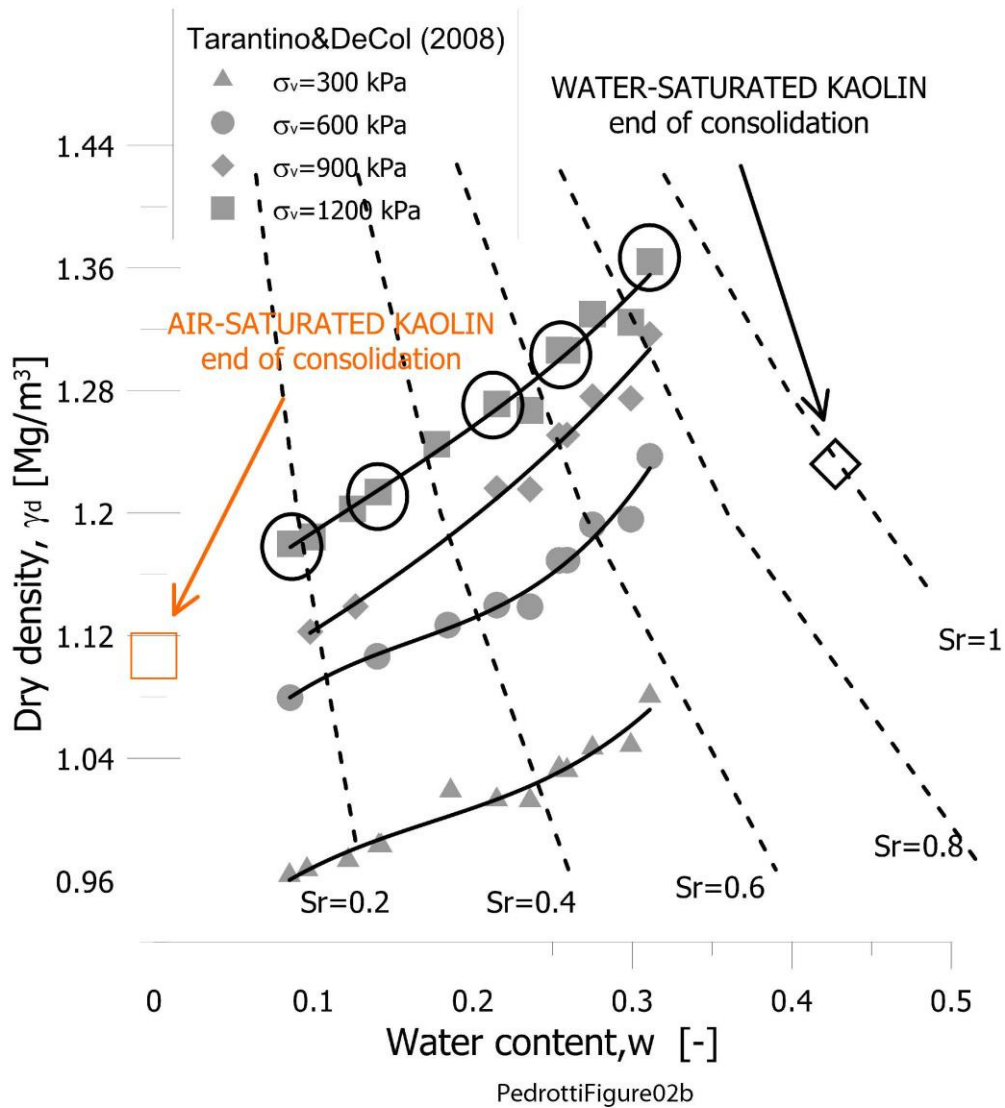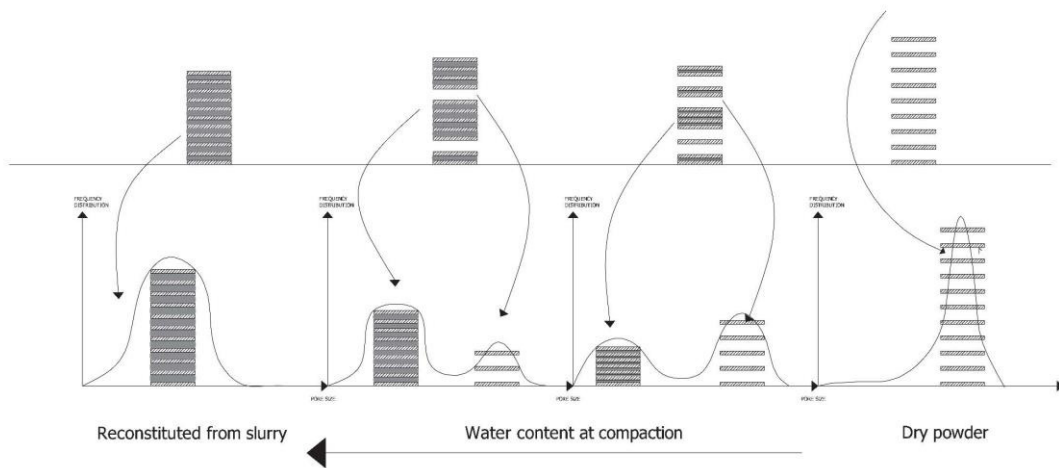
PedrottiFigure03
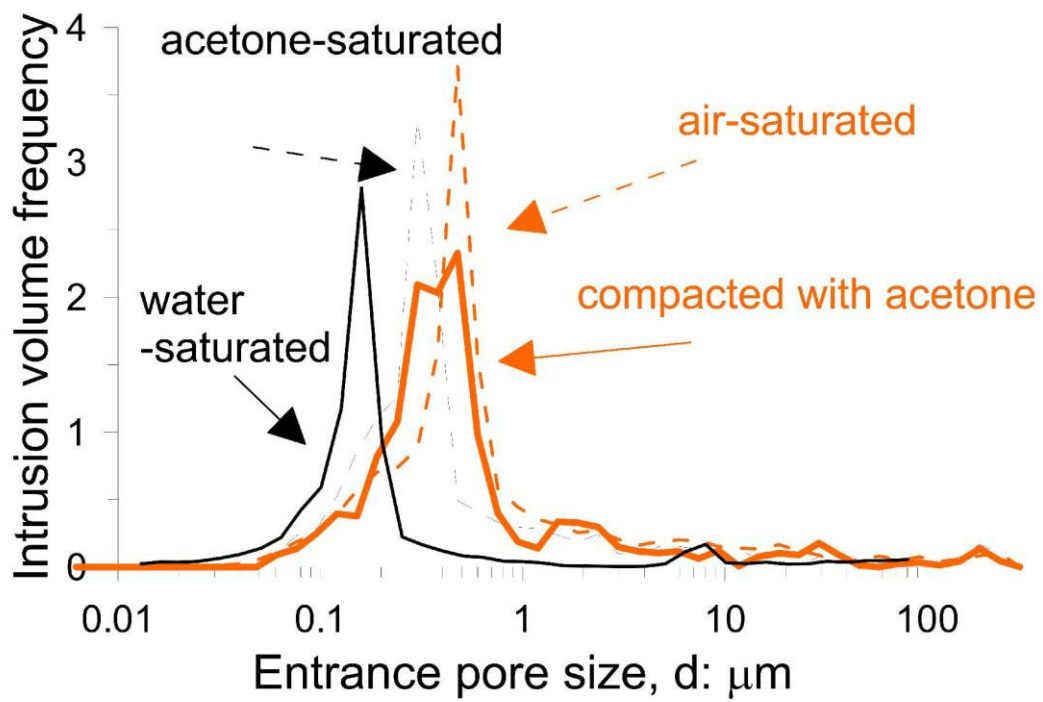
PedrottiFigure04a

PedrottiFigure04b
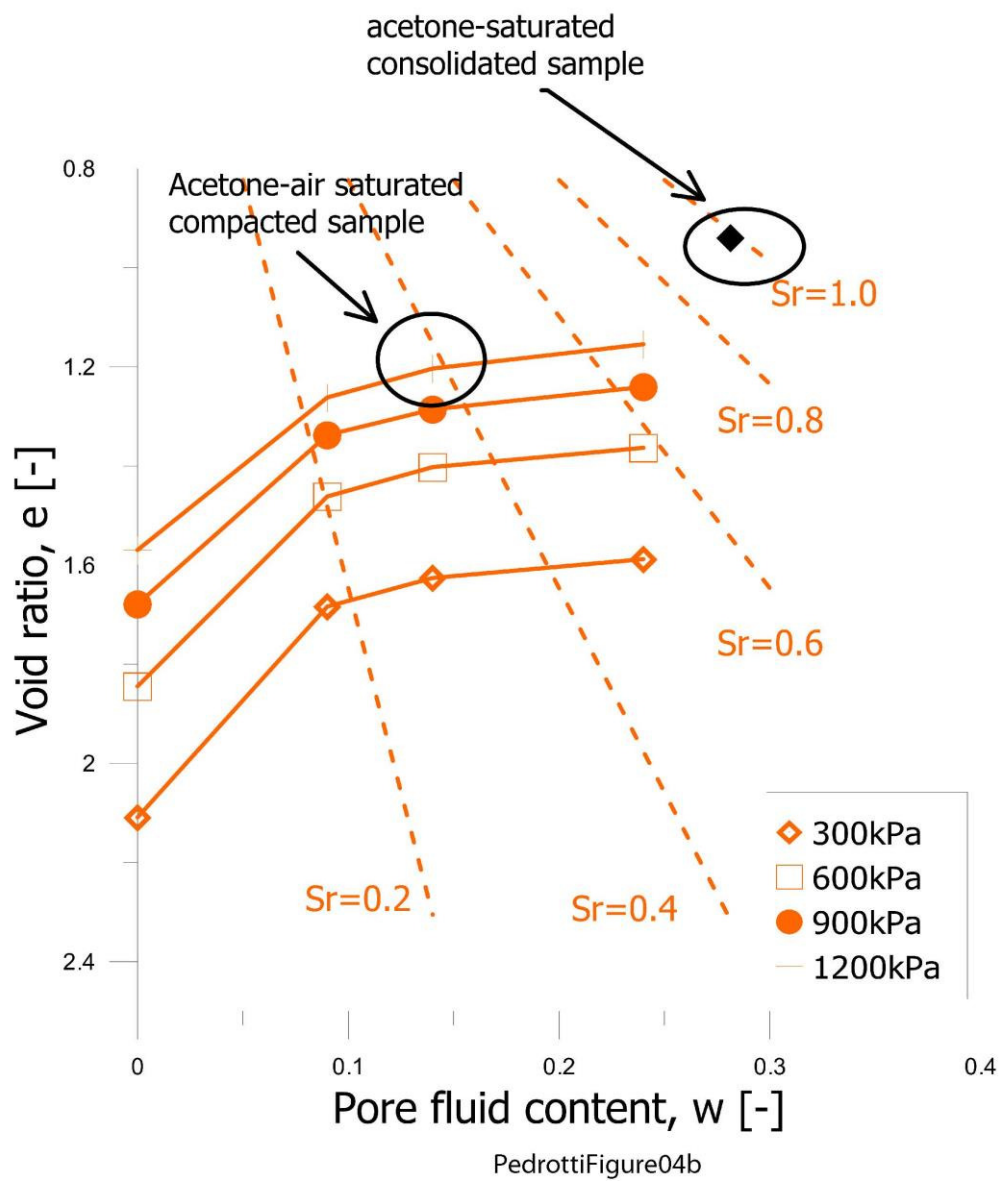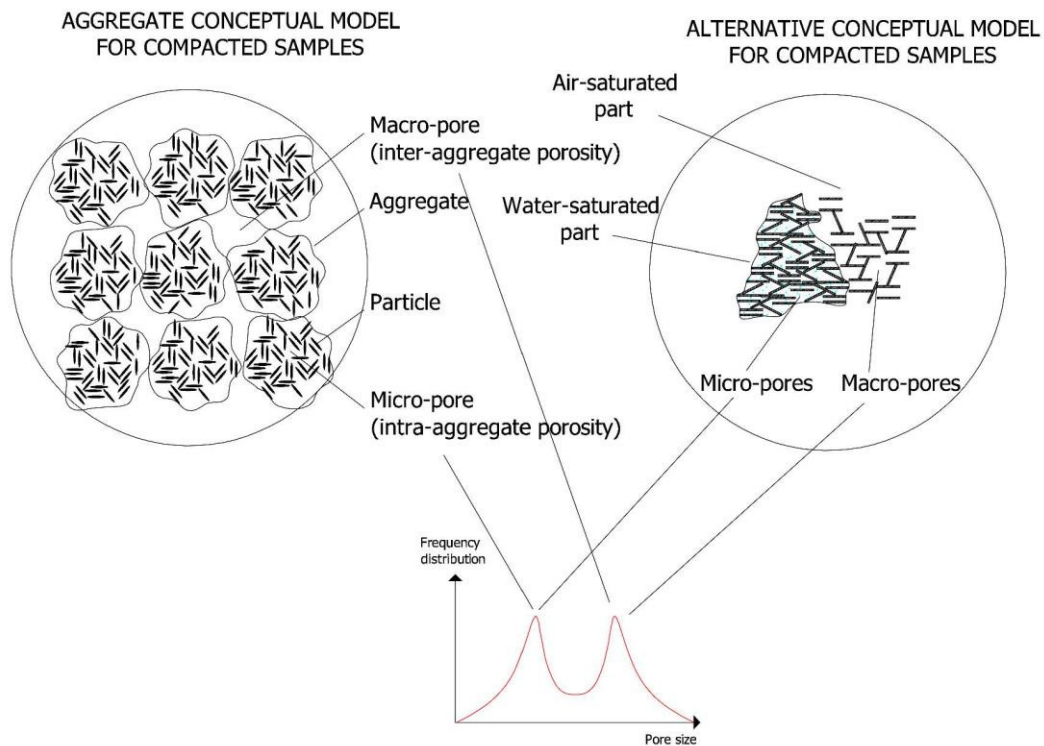
PedrottiFigure05

PedrottiFigure06

PedrottiFigure07

PedrottiFigure08a

water-
low suction

air

macro-pore

micro-pore

Wetting
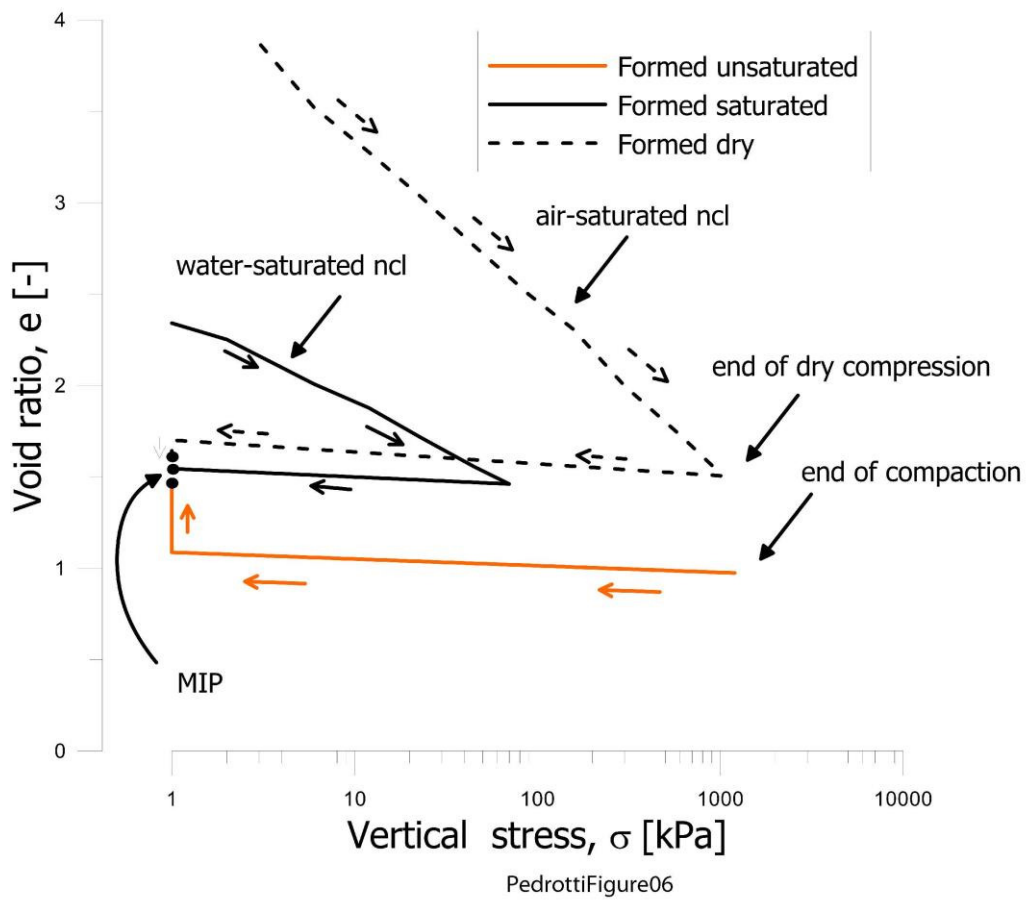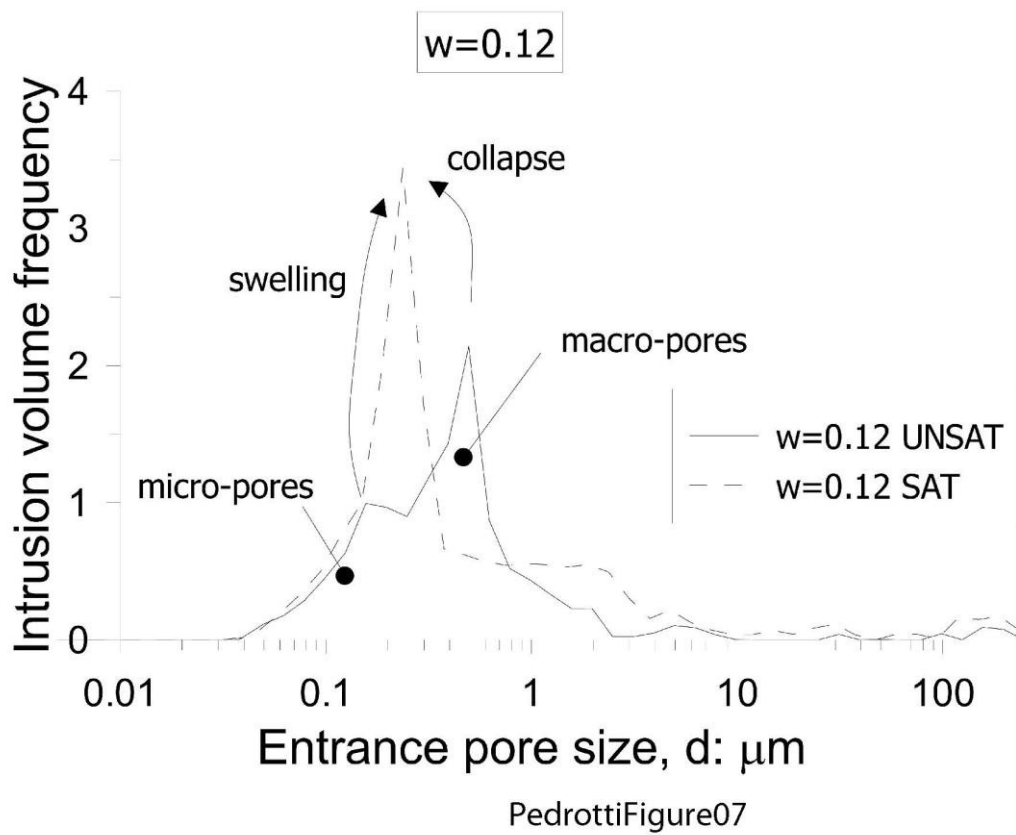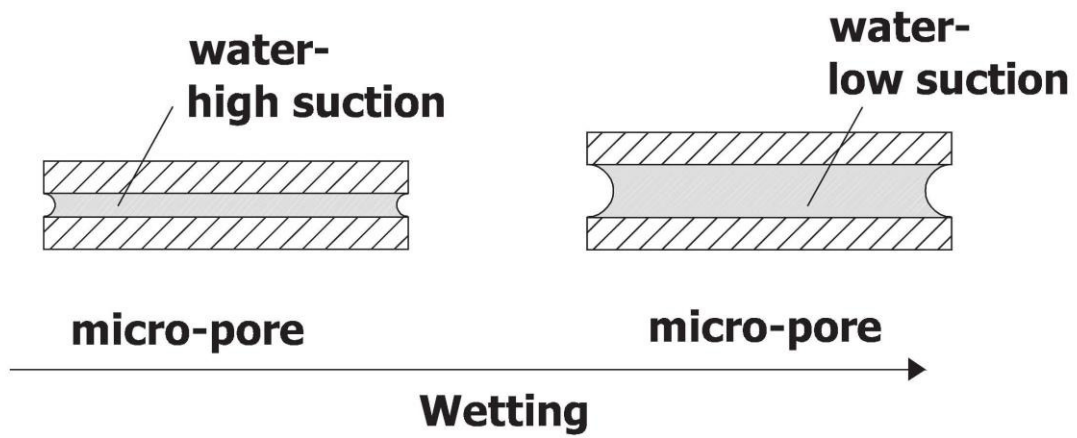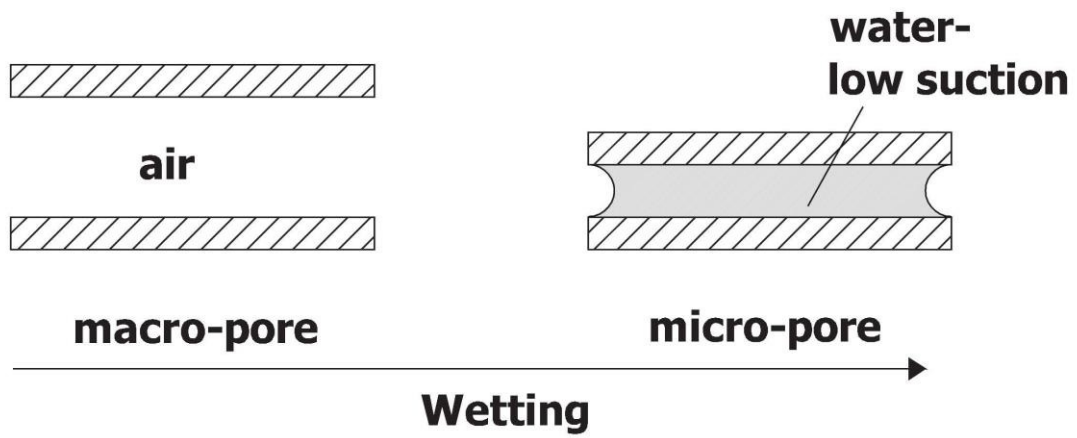
PedrottiFigure08b
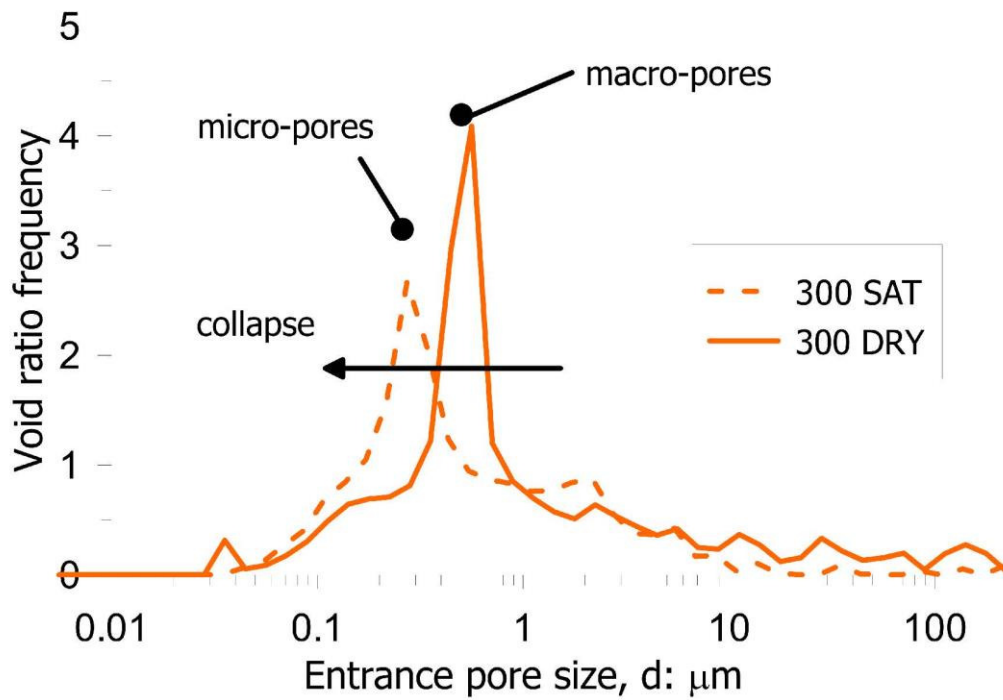
PedrottiFigure09

PedrottiFigure10

PedrottiFigure11a
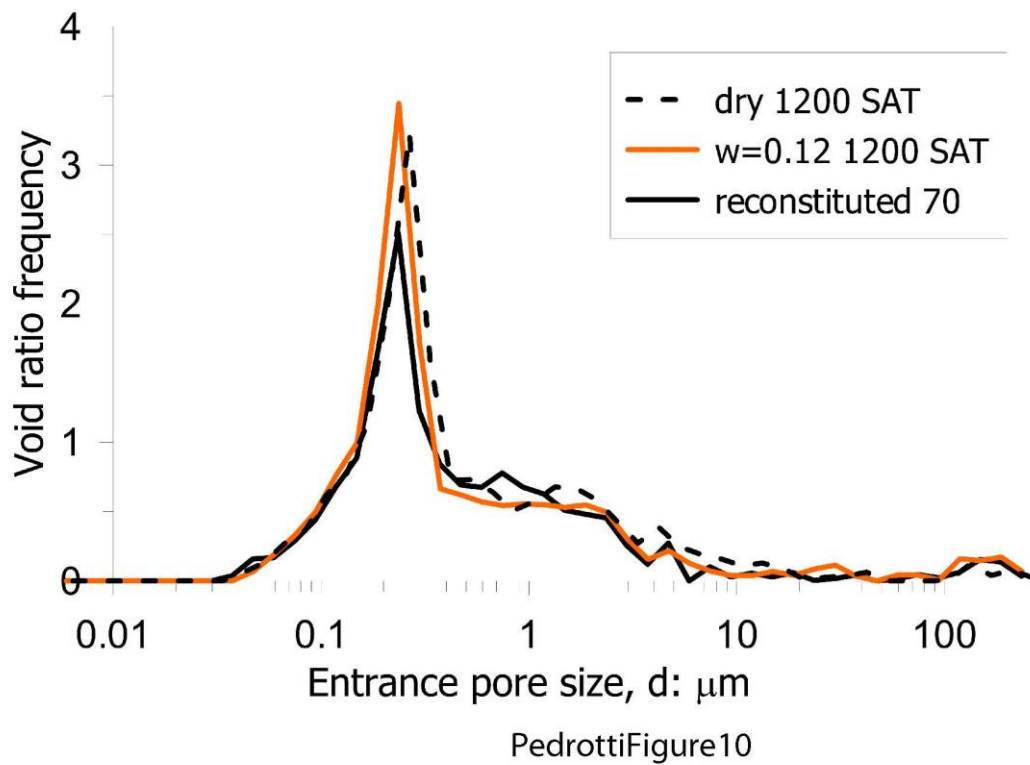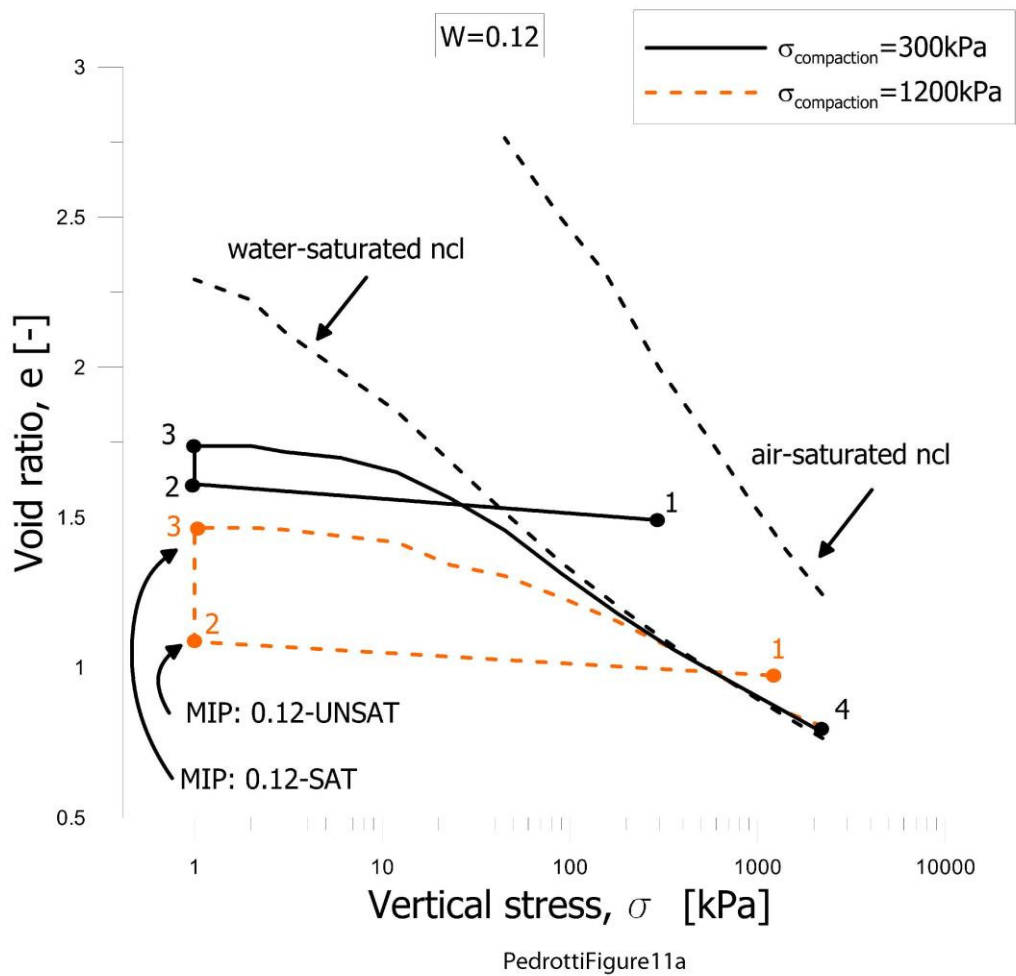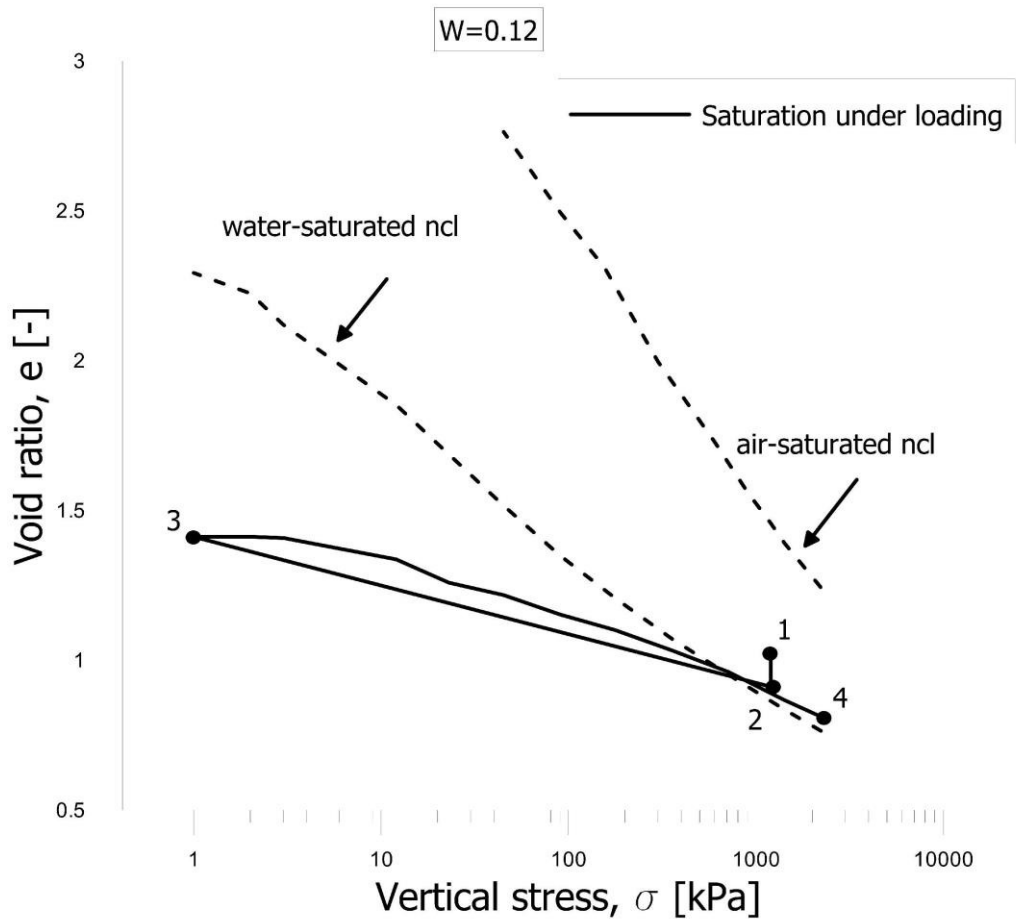
PedrottiFigure11b

PedrottiFigure12a
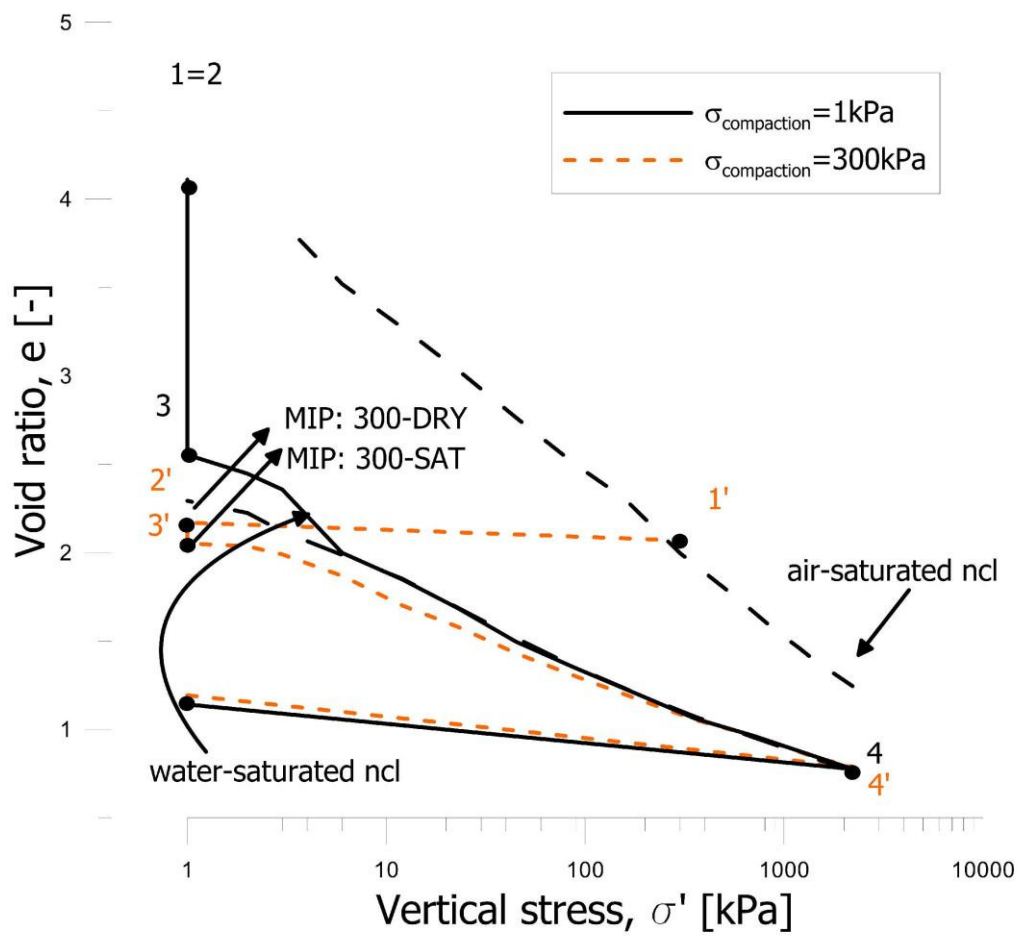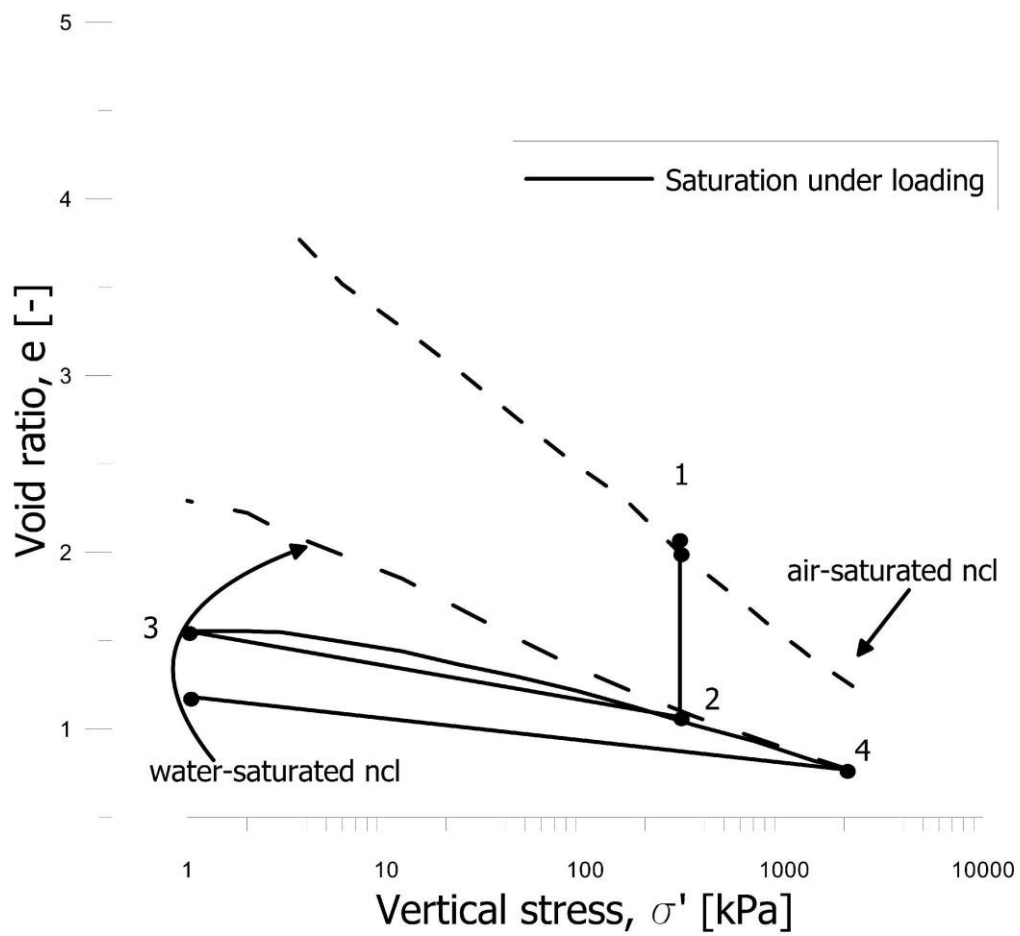
PedrottiFigure12b
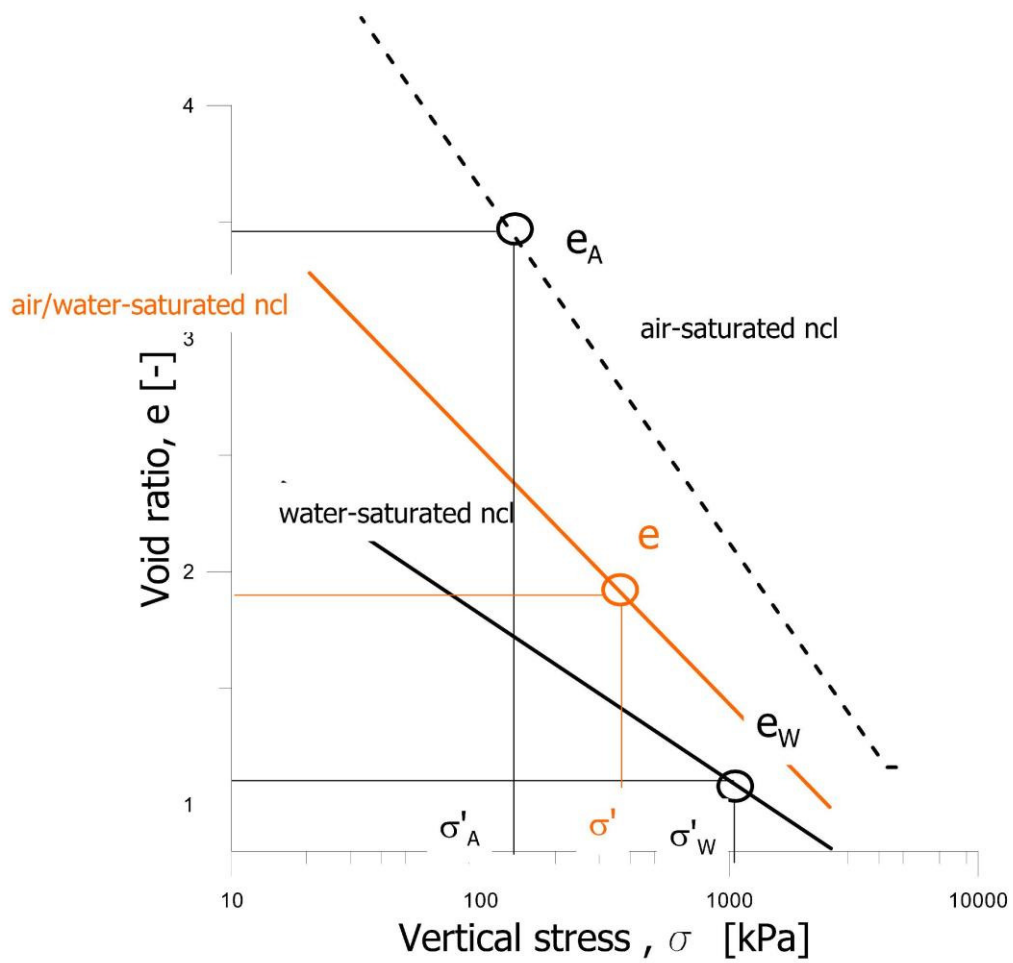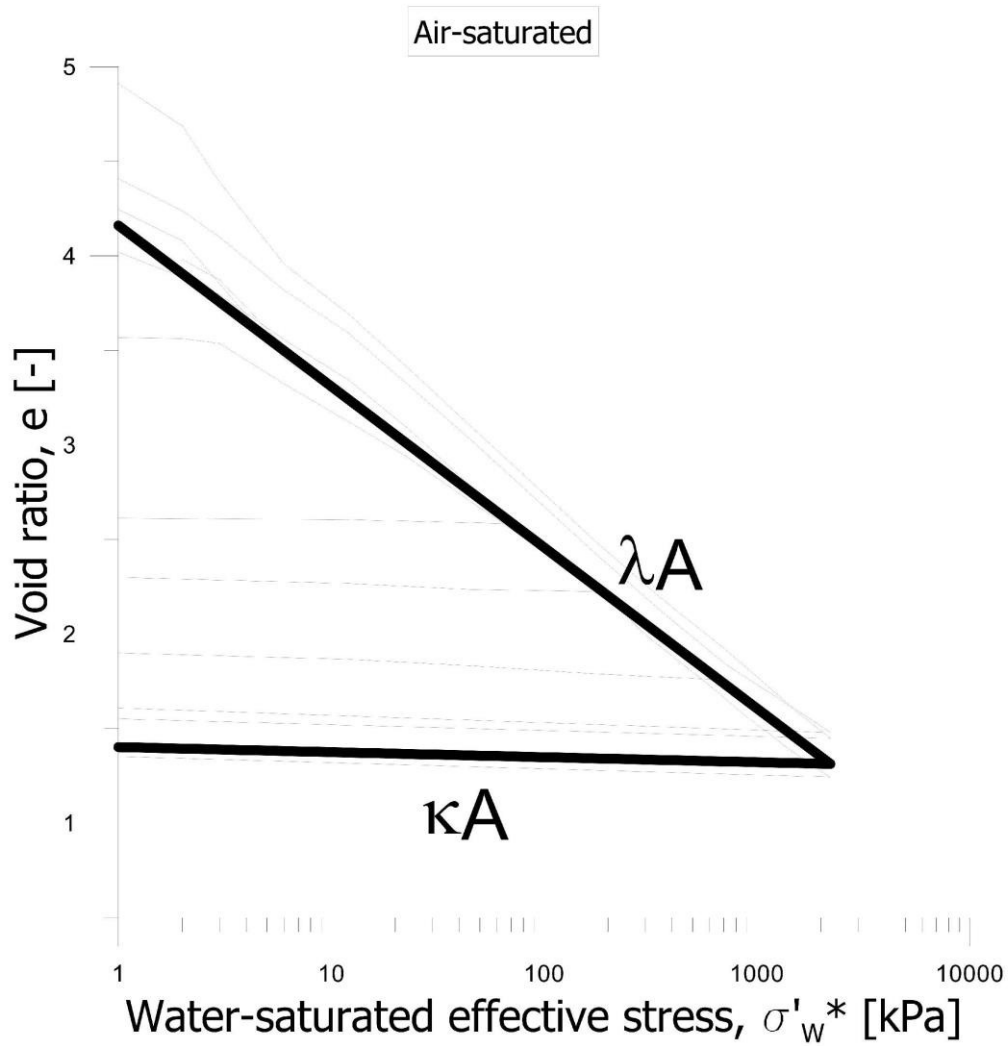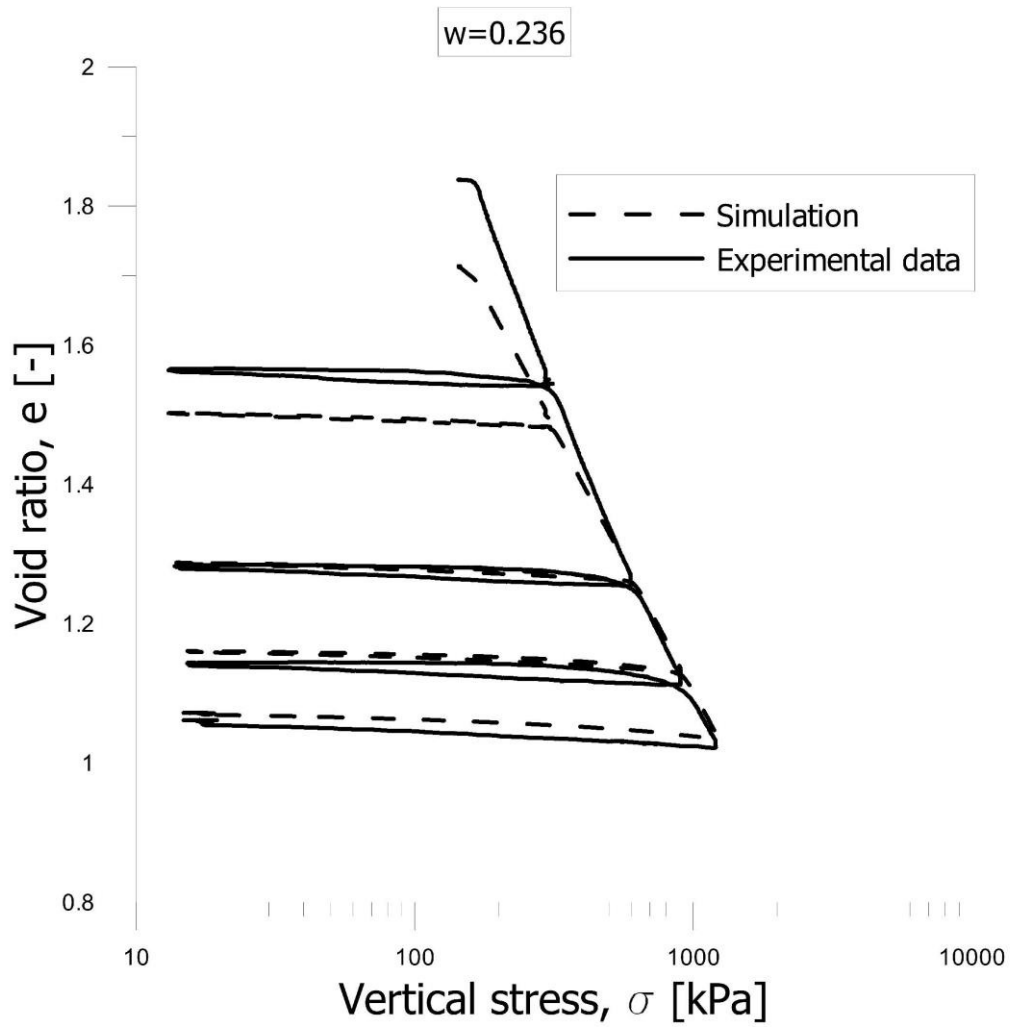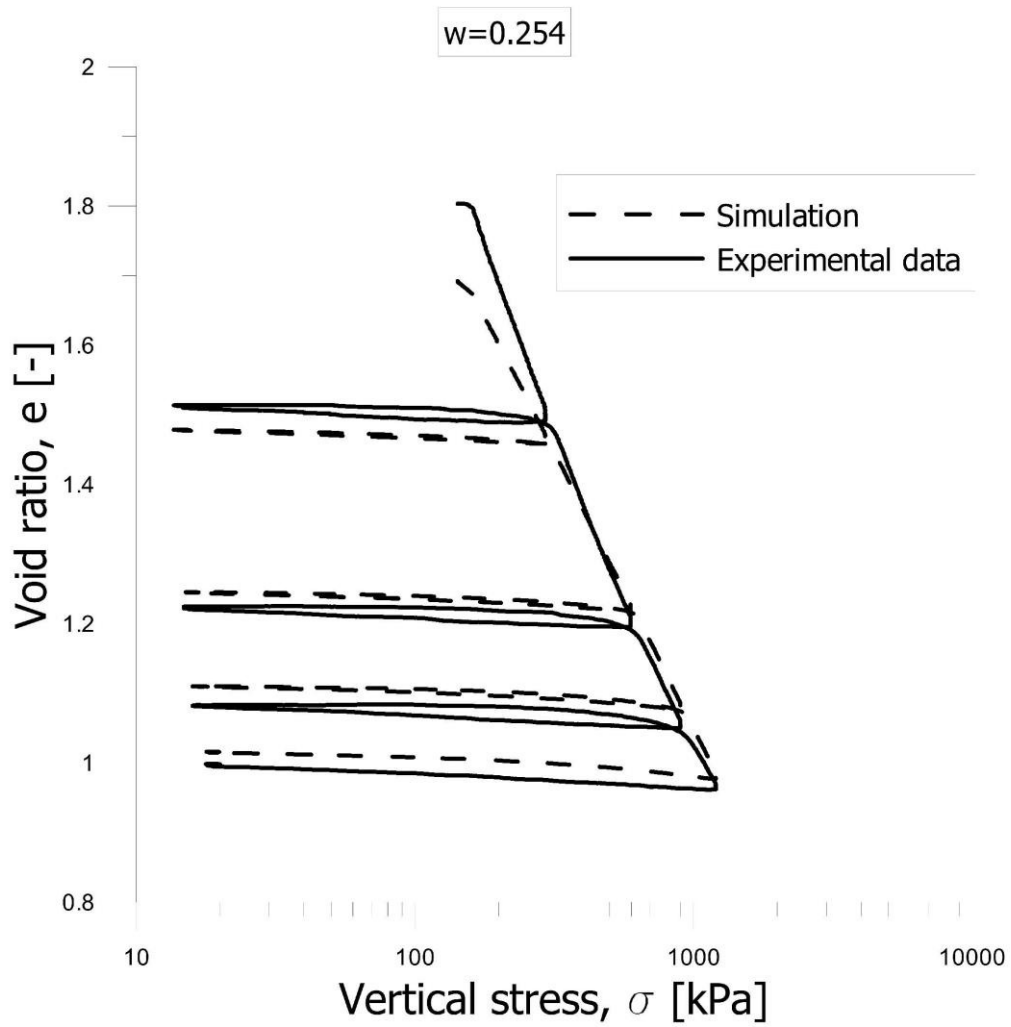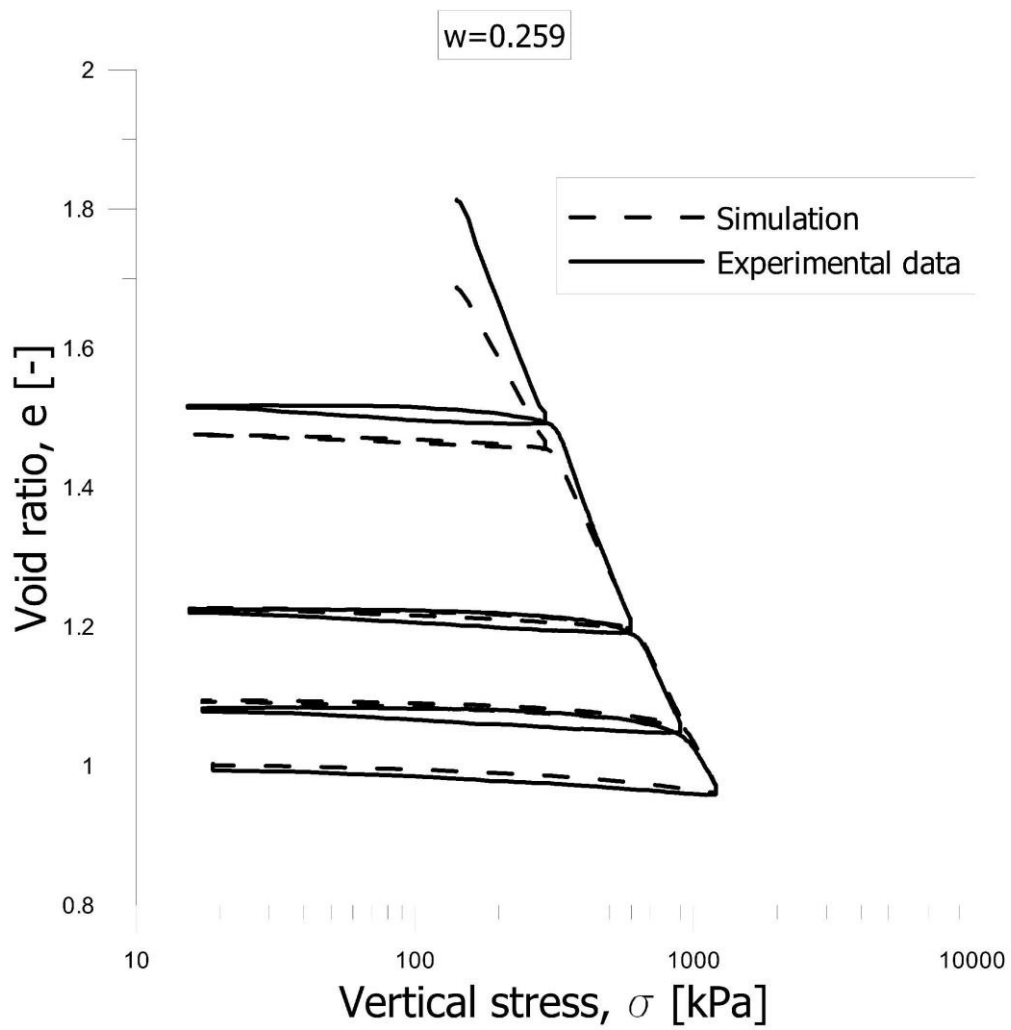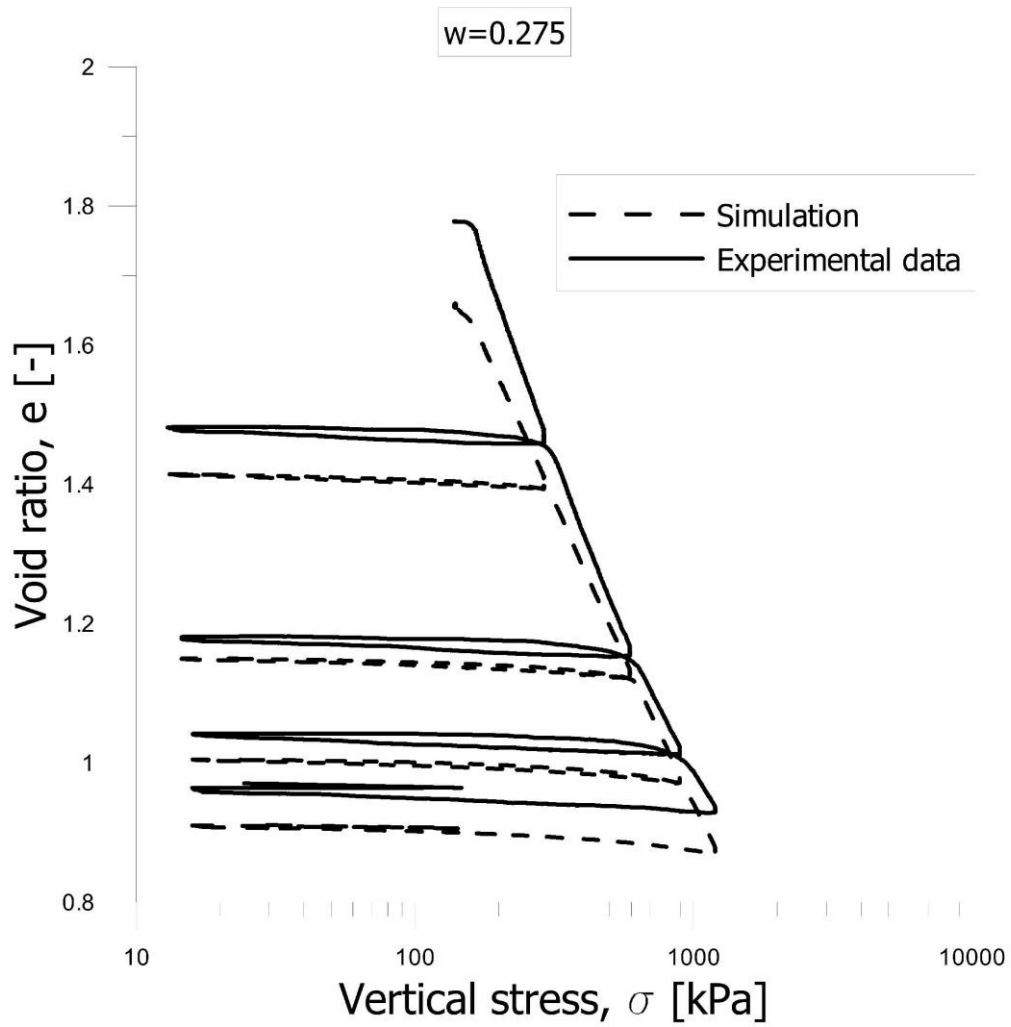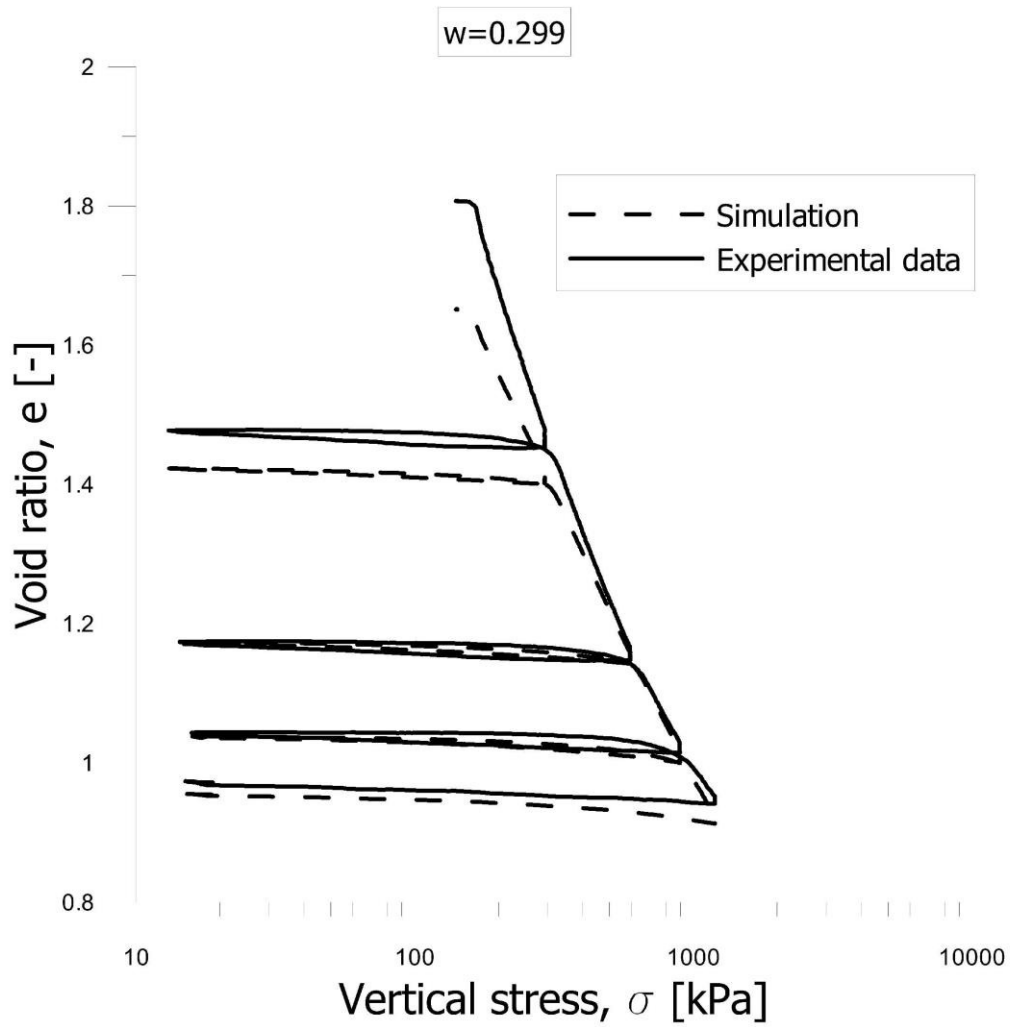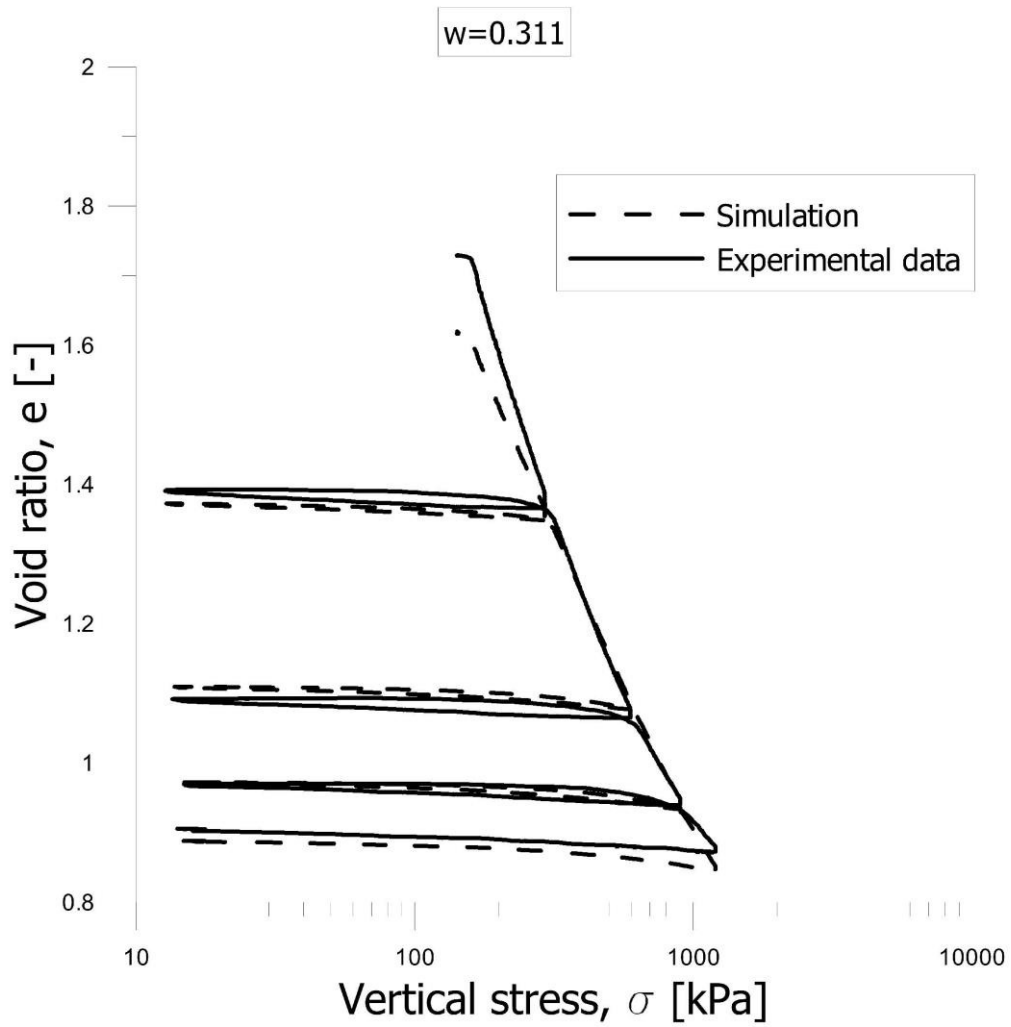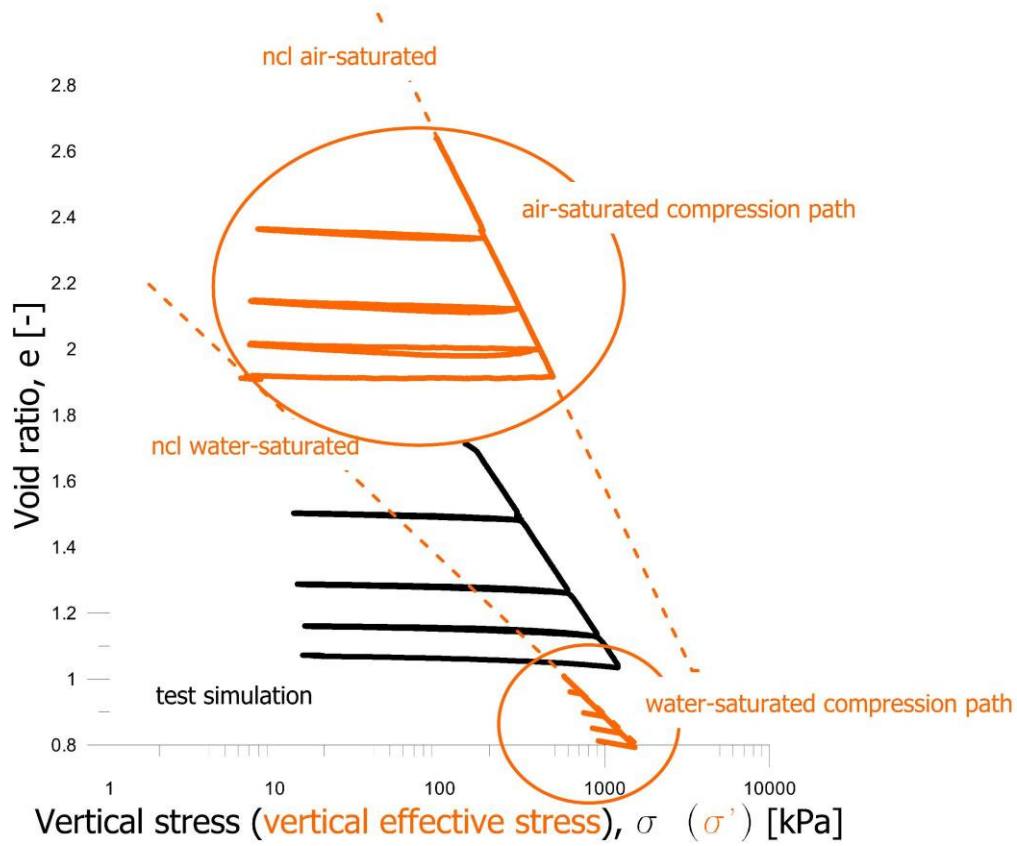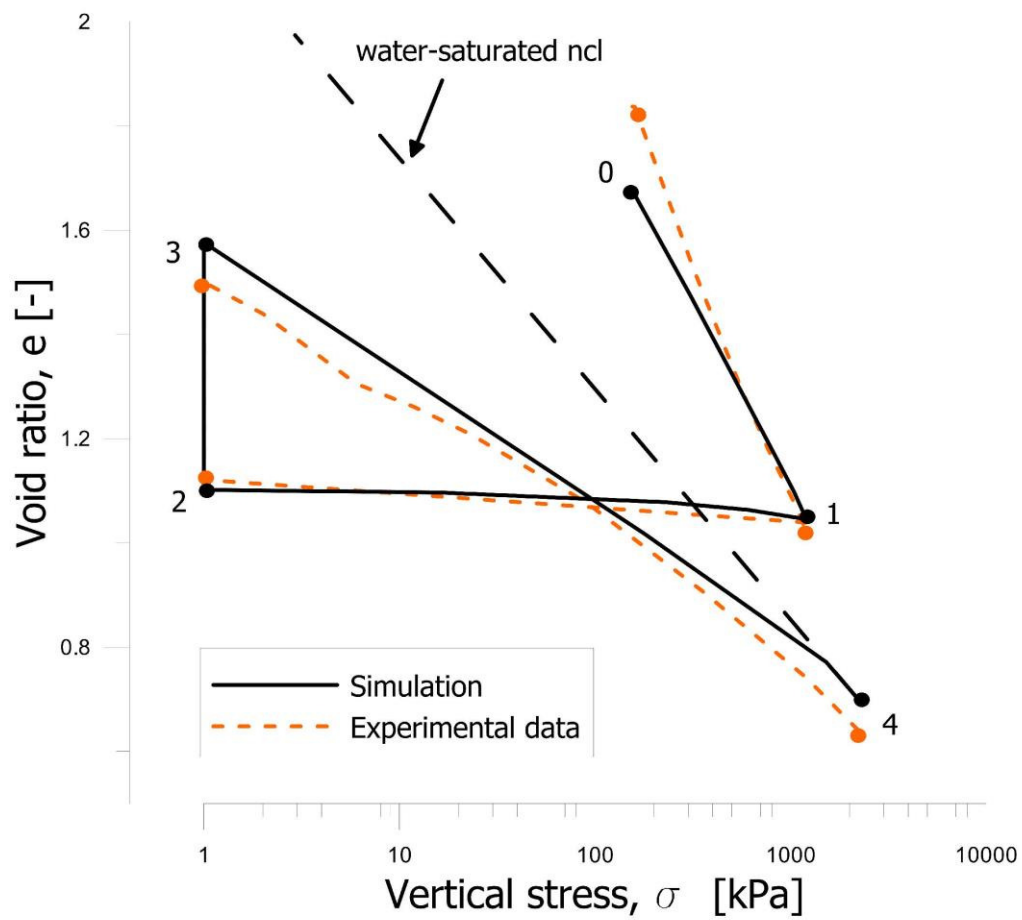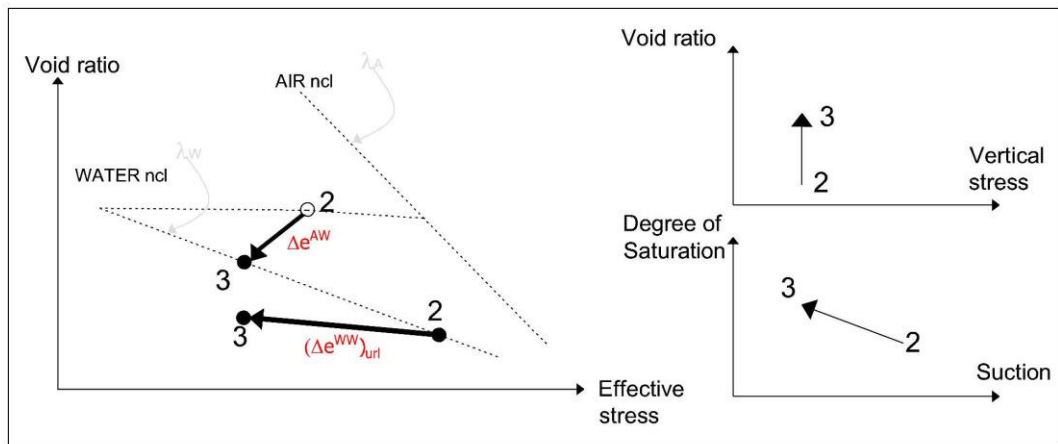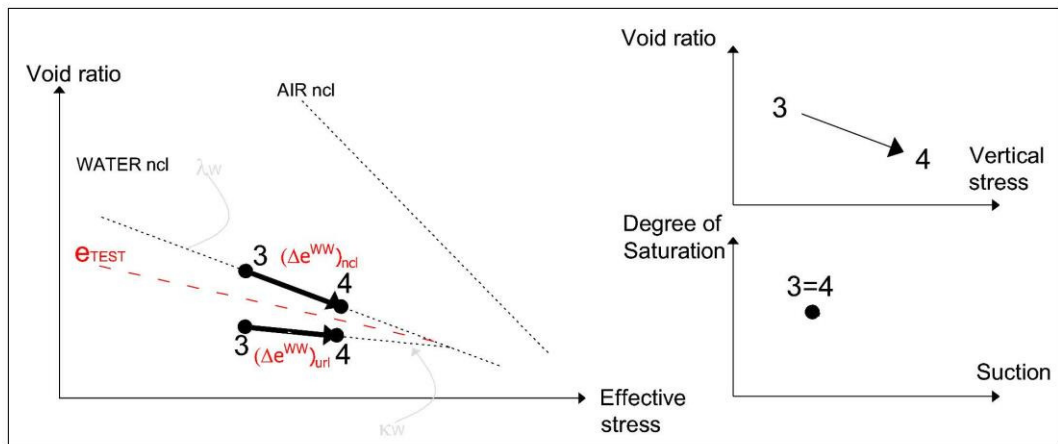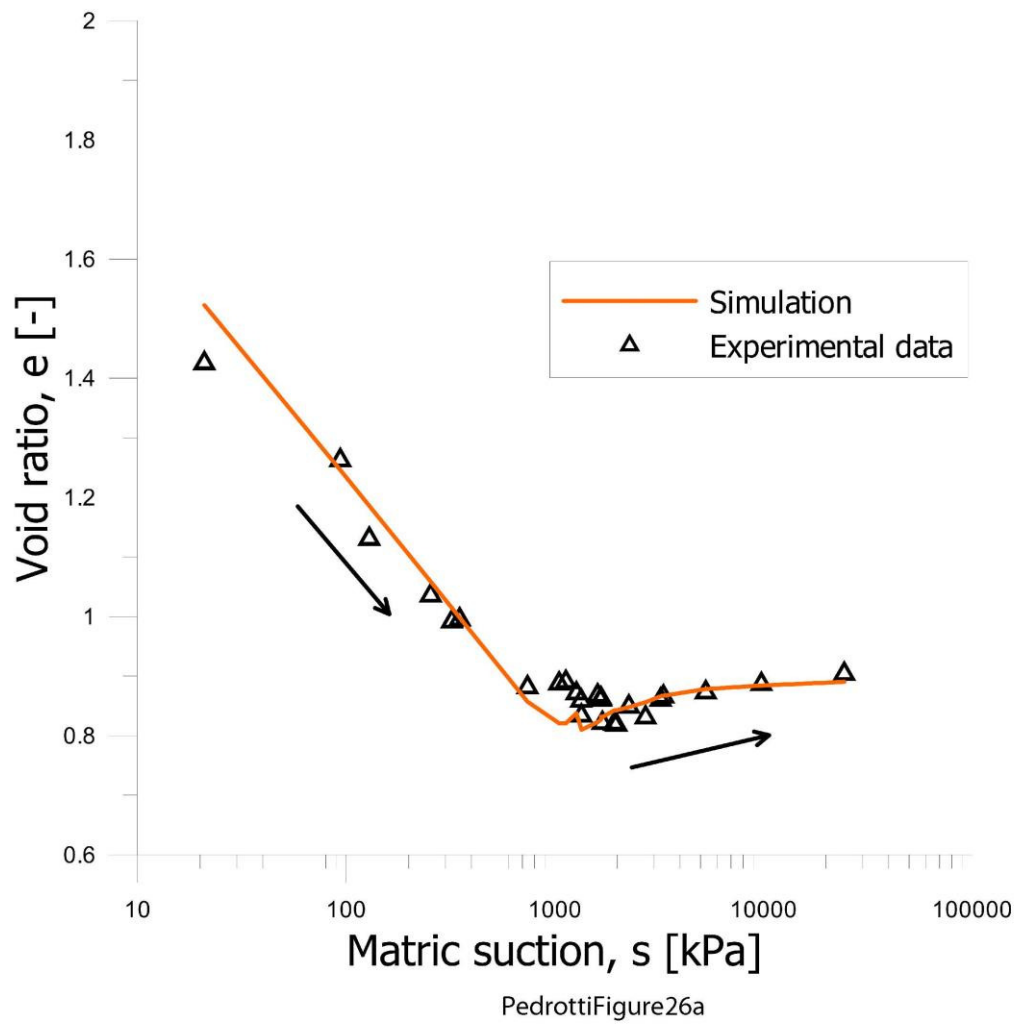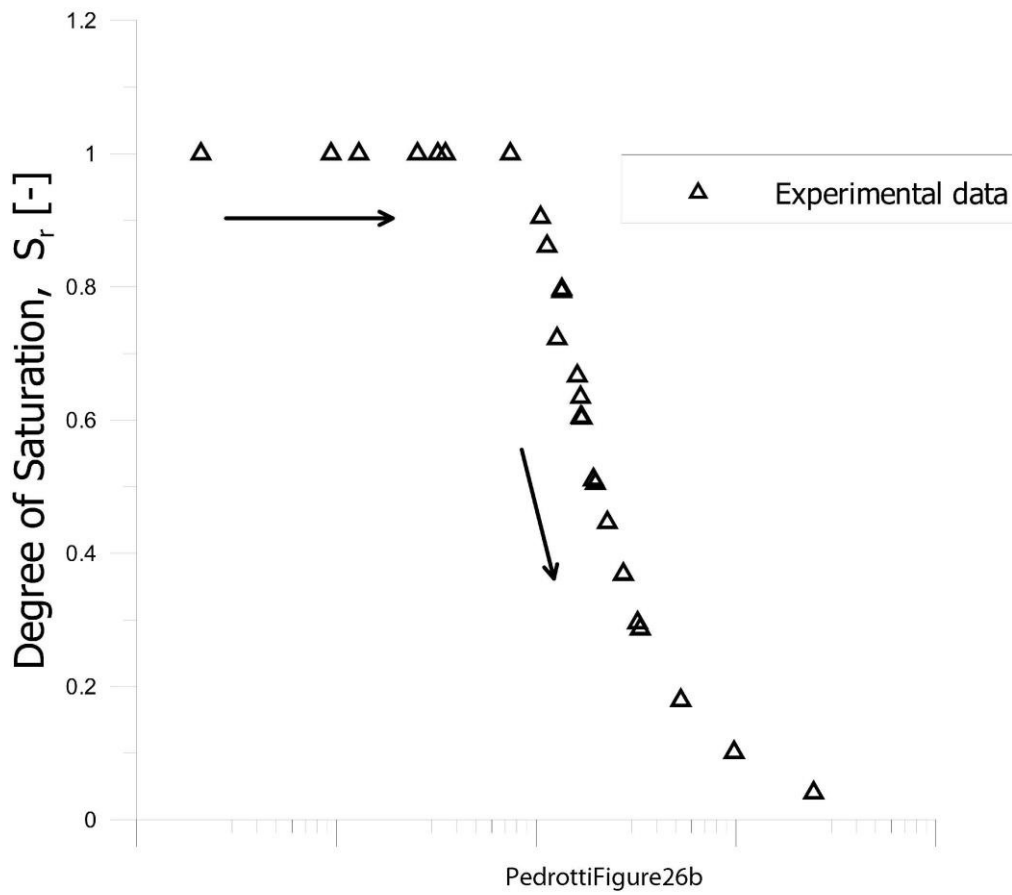
PedrottiFigure13
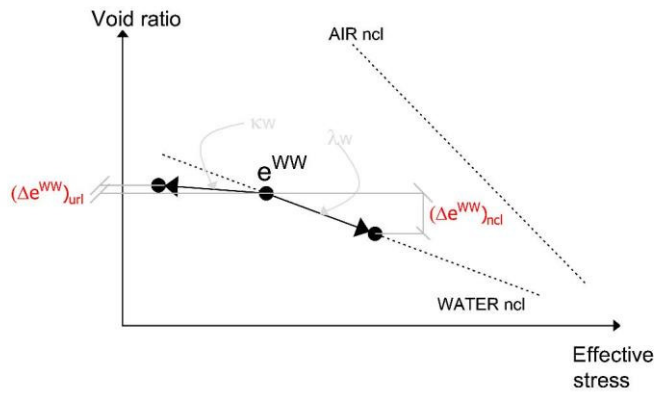
PedrottiFigure14a
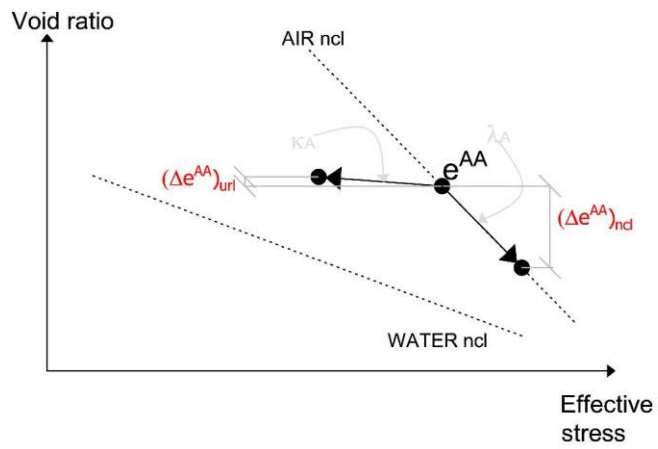
PedrottiFigure14b
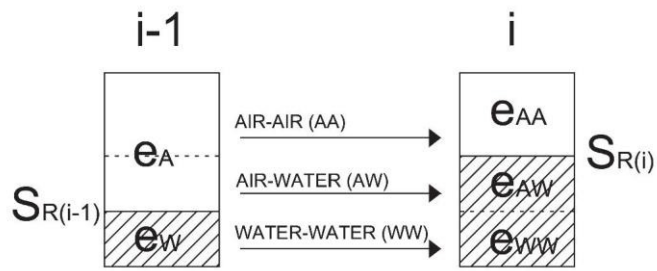
PedrottiFigure15a
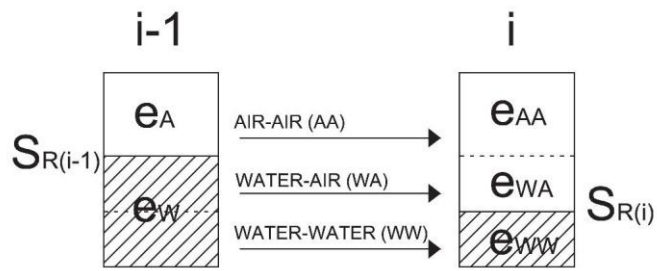
PedrottiFigure15b
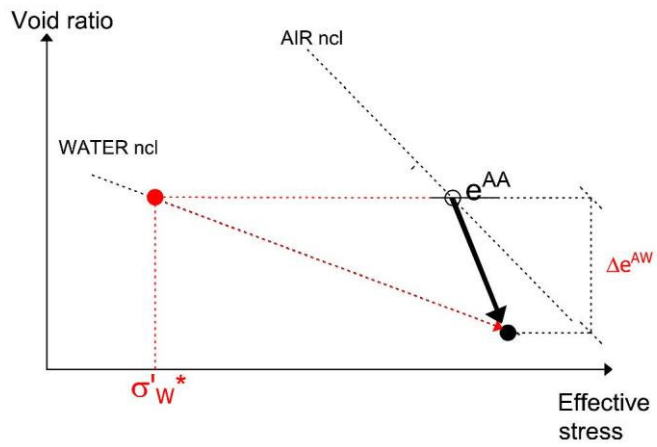
PedrottiFigure16
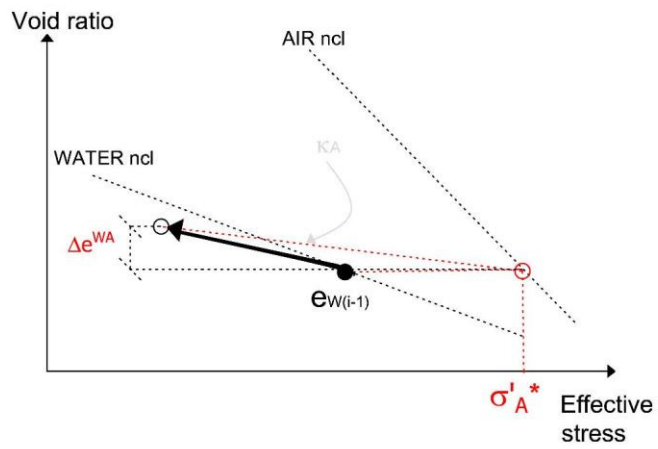
PedrottiFigure17
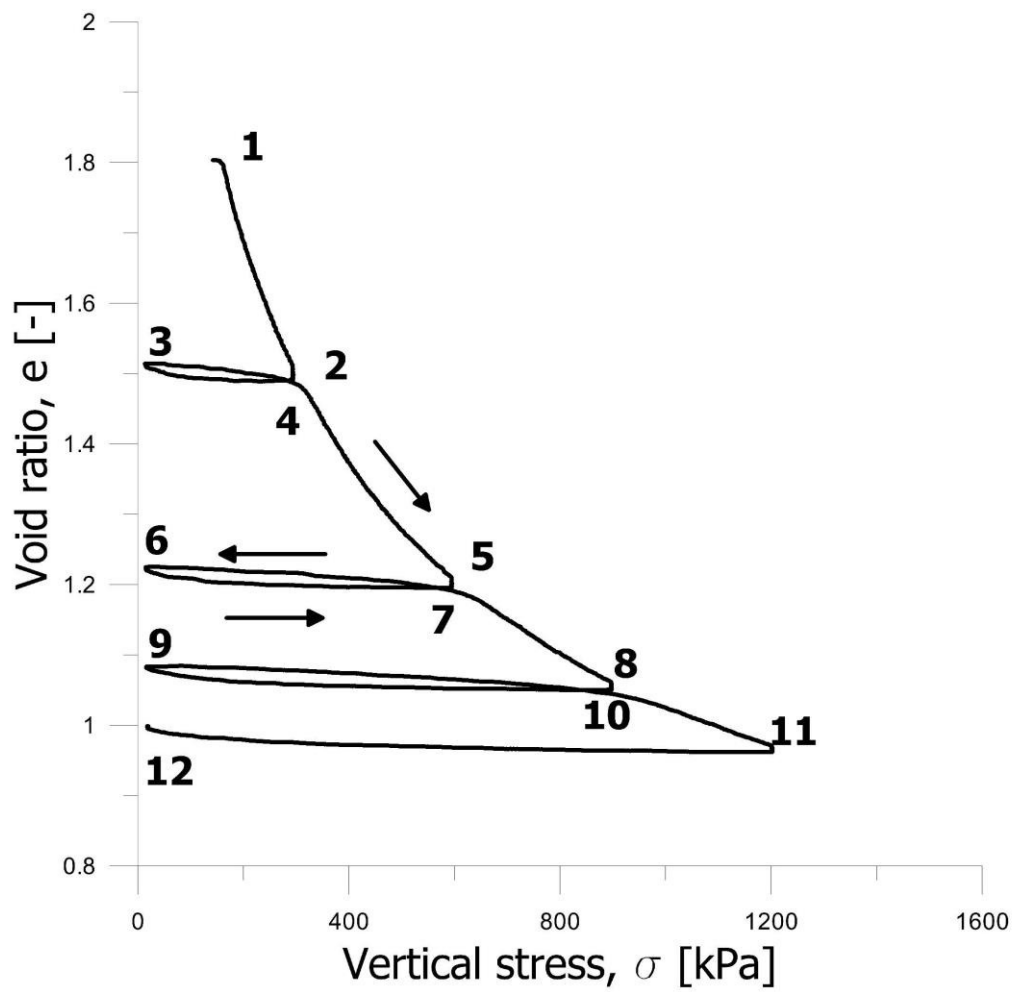
PedrottiFigure18a

PedrottiFigure18b
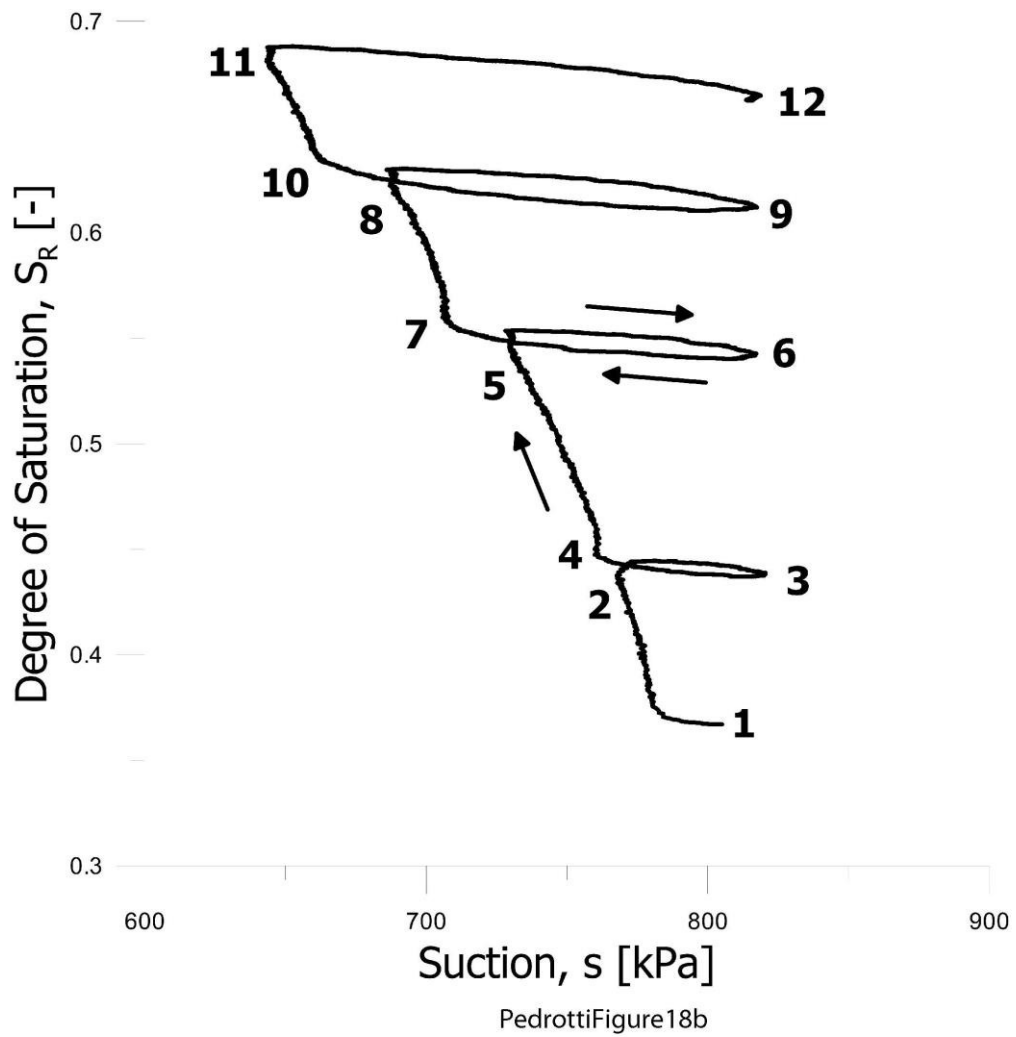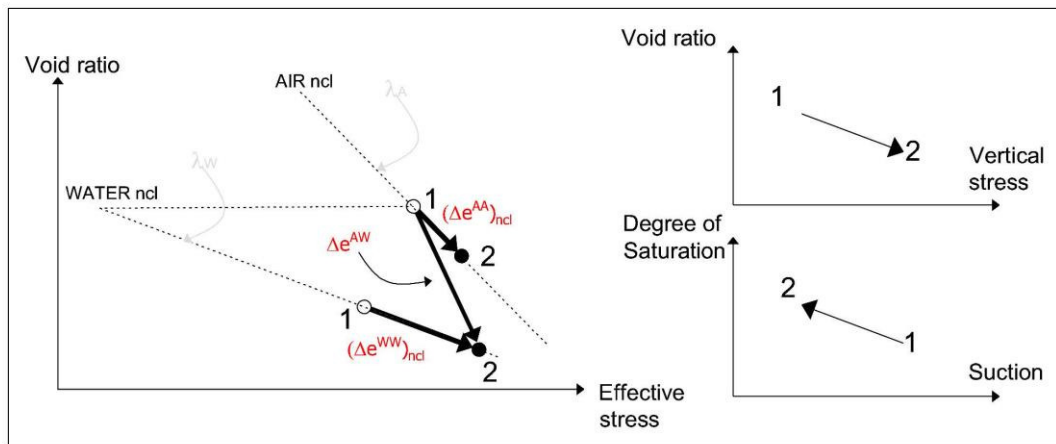
PedrottiFigure19
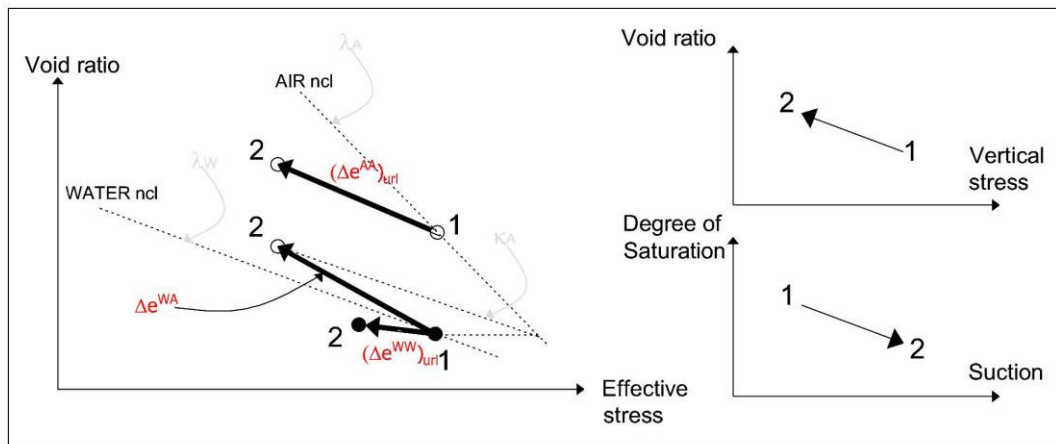
PedrottiFigure20
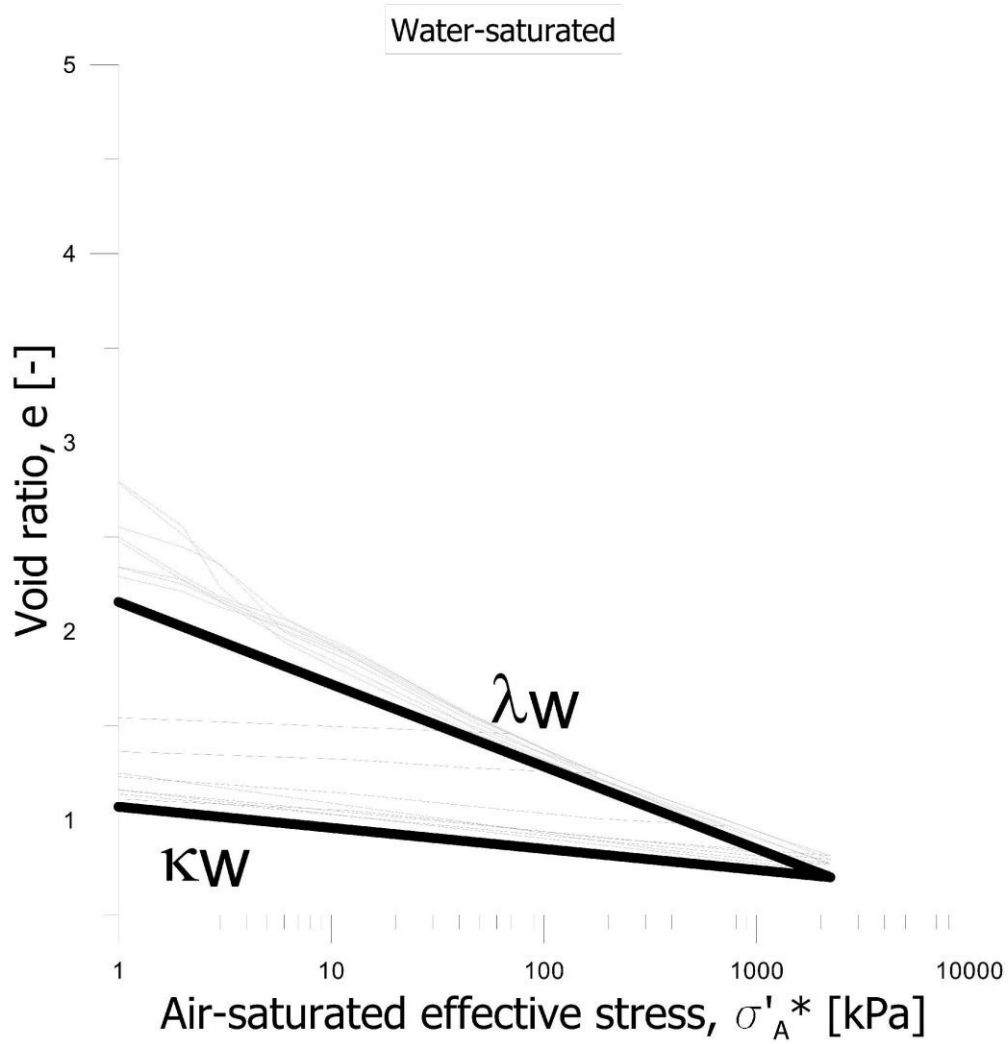
PedrottiFigure21a

PedrottiFigure21b

PedrottiFigure22a

w=0.254

PedrottiFigure22b

PedrottiFigure22c

PedrottiFigure22d

PedrottiFigure22e

w=0.311
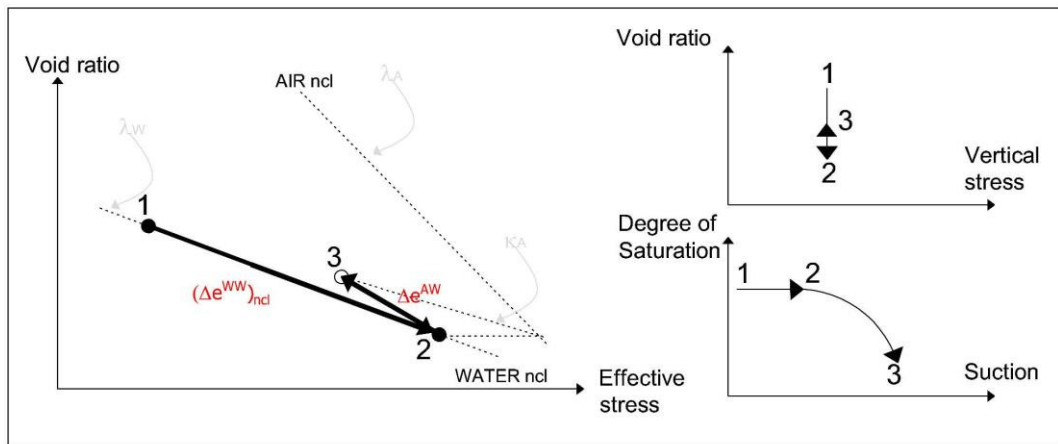
PedrottiFigure22f

PedrottiFigure23
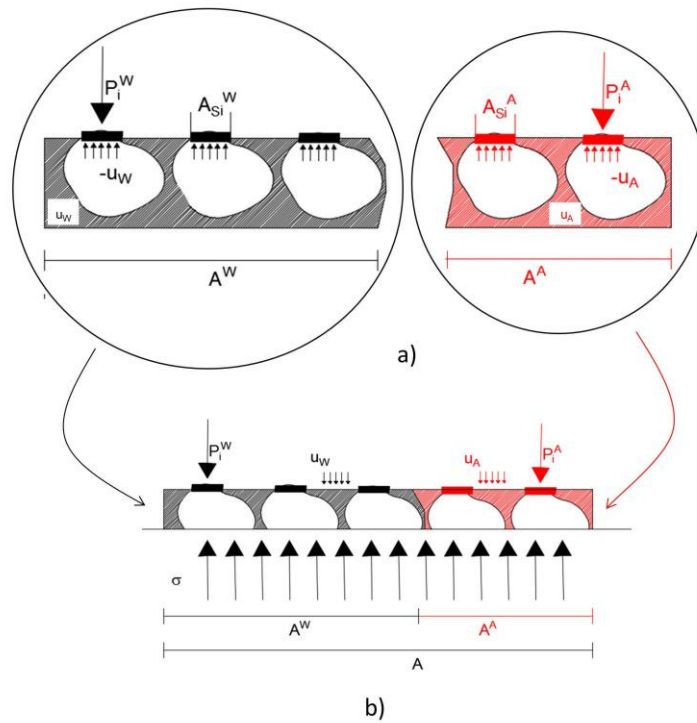
PedrottiFigure24

PedrottiFigure25a

PedrottiFigure25b

PedrottiFigure26a

PedrottiFigure26b

PedrottiFigure27

PedrottiFigure28